



UNIVERSITY OF LEEDS

This is a repository copy of *A robotic microsurgical forceps for transoral laser microsurgery*.

White Rose Research Online URL for this paper:  
<http://eprints.whiterose.ac.uk/156795/>

Version: Accepted Version

---

**Article:**

Chauhan, M [orcid.org/0000-0001-9742-5352](https://orcid.org/0000-0001-9742-5352), Deshpande, N, Pacchierotti, C et al. (4 more authors) (2019) *A robotic microsurgical forceps for transoral laser microsurgery*. *International Journal of Computer Assisted Radiology and Surgery*, 14 (2). pp. 321-333. ISSN 1861-6410

<https://doi.org/10.1007/s11548-018-1887-3>

---

© 2018, Springer Nature. This is an author produced version of an article published in *International Journal of Computer Assisted Radiology and Surgery*. Uploaded in accordance with the publisher's self-archiving policy.

**Reuse**

Items deposited in White Rose Research Online are protected by copyright, with all rights reserved unless indicated otherwise. They may be downloaded and/or printed for private study, or other acts as permitted by national copyright laws. The publisher or other rights holders may allow further reproduction and re-use of the full text version. This is indicated by the licence information on the White Rose Research Online record for the item.

**Takedown**

If you consider content in White Rose Research Online to be in breach of UK law, please notify us by emailing [eprints@whiterose.ac.uk](mailto:eprints@whiterose.ac.uk) including the URL of the record and the reason for the withdrawal request.



[eprints@whiterose.ac.uk](mailto:eprints@whiterose.ac.uk)  
<https://eprints.whiterose.ac.uk/>

# International Journal of Computer Assisted Radiology and Surgery

## A Robotic Microsurgical Forceps for Transoral Laser Microsurgery

--Manuscript Draft--

<b>Manuscript Number:</b>	CARS-D-18-00244
<b>Full Title:</b>	A Robotic Microsurgical Forceps for Transoral Laser Microsurgery
<b>Article Type:</b>	Original Article
<b>Keywords:</b>	Robot-assisted microsurgical forceps; robotic teleoperation; tissue gripping haptic feedback; robotic medical instruments; minimally invasive surgery; transoral laser microsurgery
<b>Corresponding Author:</b>	Nikhil Deshpande, Ph.D. Istituto Italiano di Tecnologia Genova, ITALY
<b>Corresponding Author Secondary Information:</b>	
<b>Corresponding Author's Institution:</b>	Istituto Italiano di Tecnologia
<b>Corresponding Author's Secondary Institution:</b>	
<b>First Author:</b>	Manish Chauhan
<b>First Author Secondary Information:</b>	
<b>Order of Authors:</b>	Manish Chauhan Nikhil Deshpande, Ph.D. Claudio Pacchierotti Leonardo Meli Domenico Prattichizzo Darwin G. Caldwell Leonardo S. Mattos
<b>Order of Authors Secondary Information:</b>	
<b>Funding Information:</b>	
<b>Abstract:</b>	<p><b>Purpose:</b> In Transoral Laser Microsurgery (TLM), the close curved cylindrical structure of the laryngeal region offers functional challenges to surgeons who operate on its malignancies with rigid, single degree-of-freedom (DOF) forceps. These challenges include surgeon hand tremors, poor reachability, poor tissue surface perception, and reduced ergonomics in design. The integrated robotic microsurgical forceps presented here, is capable of addressing the above challenges through tele-operated tissue manipulation in TLM.</p> <p><b>Methods:</b> The proposed device is designed in compliance with the spatial constraints in TLM. It incorporates a novel 2-DOF motorized microsurgical forceps end-effector, which is integrated with a commercial 6-DOF serial robotic manipulator. The integrated device is tele-operated through the haptic master interface, Omega.7. The device is augmented with a force sensor measuring tissue gripping force. The device is referred to as RMF-2F, i.e., robotic microsurgical forceps with 2-DOF end-effector and force sensing.</p> <p>RMF-2F is evaluated through validation trials and pick-n-place experiments with subjects. Furthermore, the device is trialed with expert surgeons through preliminary tasks in a simulated surgical scenario.</p> <p><b>Results:</b> RMF-2F shows a motion tracking error of less than 400µm. User trials demonstrate the device's accuracy in task completion and ease of manoeuvrability using the Omega.7 through improved trajectory following and execution times. The tissue gripping force shows better regulation with haptic feedback (1.624 N) than without haptic feedback (2.116 N).</p>

Surgeons positively evaluated the device with appreciation for improved access in the larynx and gripping force feedback.

Conclusions: RMF-2F offers an ergonomic and intuitive interface for intraoperative tissue manipulation in TLM. The device performance, usability, and haptic feedback capability were positively evaluated by users as well as expert surgeons. RMF-2F introduces the benefits of robotic teleoperation including, (i) overcoming hand tremors and wrist excursions, (ii) improved reachability and accuracy, and (iii) tissue gripping feedback for safe tissue manipulation.

[Click here to view linked References](#)

**Title:** A Robotic Microsurgical Forceps for Transoral Laser Microsurgery

**Authors:** Manish Chauhan<sup>1</sup>, Nikhil Deshpande<sup>2</sup>, Claudio Pacchierotti<sup>3</sup>, Leonardo Meli<sup>4</sup>, Domenico Prattichizzo<sup>2,4</sup>, Darwin G. Caldwell<sup>2</sup>, Leonardo S. Mattos<sup>2</sup>.

**Affiliations:** (1) STORM Lab, School of Electronics and Electrical Engineering, University of Leeds, LS2 9JT, UK. (2) Department of Advanced Robotics, Istituto Italiano di Tecnologia, Via Morego 30, 16163, Genova, Italy. (3) CNRS, Univ Rennes, Inria, IRISA, Campus Universitaire de Beaulieu, 35042 Rennes, France. (4) Department of Information Engineering and Mathematics, Università degli Studi di Siena, Via Roma 56, 53100 Siena, Italy.

**Site of research and experiments:** The research was carried out at the Istituto Italiano di Tecnologia (IIT) in Genova, Italy.

**Funding:** The study did not receive any external funding.

**Conflict of Interest:** The authors declare that they have no conflict of interest.

**Ethical approval:** For this type of study, formal consent was not required. The Ethics Committee of Liguria Region granted the exemption for the use of human subjects and ex-vivo pig larynxes for the trials.

**Informed consent:** Informed consent was obtained from all individual participants included in the study.

**Corresponding Author:** Nikhil Deshpande, Department of Advanced Robotics, Istituto Italiano di Tecnologia, Via Morego 30, 16163, Genova, Italy. Email: [nikhil.deshpande@iit.it](mailto:nikhil.deshpande@iit.it). Ph: (+39) 010 71781 805.

## **Abstract:**

**Purpose:** In Transoral Laser Microsurgery (TLM), the close curved cylindrical structure of the laryngeal region offers functional challenges to surgeons who operate on its malignancies with rigid, single degree-of-freedom (DOF) forceps. These challenges include surgeon hand tremors, poor reachability, poor tissue surface perception, and reduced ergonomics in design. The integrated robotic microsurgical forceps presented here, is capable of addressing the above challenges through tele-operated tissue manipulation in TLM.

**Methods:** The proposed device is designed in compliance with the spatial constraints in TLM. It incorporates a novel 2-DOF motorized microsurgical forceps end-effector, which is integrated with a commercial 6-DOF serial robotic manipulator. The integrated device is tele-operated through the haptic master interface, Omega.7. The device is augmented with a force sensor measuring tissue gripping force. The device is referred to as RMF-2F, i.e., robotic microsurgical forceps with 2-DOF end-effector and force sensing.

RMF-2F is evaluated through validation trials and pick-n-place experiments with subjects. Furthermore, the device is trialled with expert surgeons through preliminary tasks in a simulated surgical scenario.

**Results:** RMF-2F shows a motion tracking error of less than 400 $\mu$ m. User trials demonstrate the device's accuracy in task completion and ease of manoeuvrability using the Omega.7 through improved trajectory following and execution times. The tissue gripping force shows better regulation with haptic feedback (1.624 N) than without haptic feedback (2.116 N).

Surgeons positively evaluated the device with appreciation for improved access in the larynx and gripping force feedback.

**Conclusions:** RMF-2F offers an ergonomic and intuitive interface for intraoperative tissue manipulation in TLM. The device performance, usability, and haptic feedback capability were positively evaluated by users as well as expert surgeons. RMF-2F introduces the benefits of robotic teleoperation including, (i) overcoming hand tremors and wrist excursions, (ii) improved reachability and accuracy, and (iii) tissue gripping feedback for safe tissue manipulation.

**Keywords:** Robot-assisted microsurgical forceps; robotic teleoperation; tissue gripping haptic feedback; robotic medical instruments; minimally invasive surgery; transoral laser microsurgery.

## 1. INTRODUCTION

Transoral Laser Microsurgery (TLM) is a non-invasive surgery for the treatment of laryngeal malignancies, e.g., cysts, polyps, nodules, or cancerous tumours. Introduced by Jako et al. [1], the traditional technique, as seen in Fig. 1, involves exposure of the surgical site with the use of a laryngoscope (length = 180mm, cross-section 16 X 23mm<sup>2</sup>), inserted into the patient's mouth. This allows a direct line-of-sight for the surgical microscope surgical site visualization. A laser micro-manipulator is coupled to the surgical microscope to aim a free-beam CO<sub>2</sub> surgical laser at the site. The mechanical micro-manipulator moves a beam-splitter mirror, which is aligned with the microscope line-of-sight. Manually handled microsurgical instruments are used for intraoperative tissue manipulation and extraction.

Figure 2 indicates the various dimensions of the components within the setup. As ins seen, within the standard 400mm laser focal distance between the base of the microscope and the surgical site, the micro-manipulator, and the laryngoscope occupy a length of 320~350mm. This leaves a narrow range of 50~80mm for manoeuvring the microsurgical instruments. It is evident that this requires the surgeon to have high psycho-motor skills to overcome challenges of coordination, poor ergonomics, and sub-optimal surgical site access, among others.

### 1.1 Problem Formulation

Microsurgical instruments in traditional TLM are manually handled, with scissor-like handles for open-close operation. The most common instrument is the microsurgical forceps (micro-forceps), used for: (i) tissue manipulation (grasping, orienting, removing); (ii) stretching tissue for precise laser cutting and ensuring minimal thermal damage to healthy tissue; and (iii) orienting tissue to view pathologies. Such handling of these rigid shaft tools causes: (i) constrained accessibility in the laryngeal region; (ii) unstable handling due to hand tremors and wrist excursions; and (iii) poor tissue gripping perception. This makes their usage cumbersome and non-ergonomic [2,3].

To overcome the above-mentioned limitations, robotic surgery has become a key part of the modern surgical infrastructure in recent years, a prime example of which is the da Vinci Surgical System [4]. Towards this end, in laryngeal surgery, Simaan et al. [5] presented snake-like manipulators having tip dexterity for tissue manipulation and suturing. Wang et al. [6] presented a robot-assisted master-slave system consisting of two symmetrical 9 degrees-of-freedom (DOFs) cable-driven manipulators, with quick-change interfaces for surgical tools. Rivera-Serrano et al. [7] presented a highly articulated robot in a follow-the-leader mechanism with 50

cylindrical links, controlled by a master controller. Solares and Strome [8] and Desai et al. [9] explored the utility of the da Vinci Surgical System [4] but found the size of the da Vinci tool shafts as a major limitation along with the constant changes required from the attendant during surgery. All these works seek to replace the microscope with dedicated instrument arms entering through the laryngoscope. Importantly, although targeted at laryngeal surgery, the above systems cannot be used in TLM, since there is no available access for the free-beam laser. He et al. [10] overcame this drawback through their cooperatively controlled teleoperation robot where the traditional TLM instruments can be directly attached / detached from the 3-DOF wrist of the robot itself. Their design serves as an important guidepost for the research in this paper.

On a related note, reduced tissue haptic perception is an important concern in surgery due to the introduction of robotic teleoperation. Haptic feedback is widely considered to be valuable for surgical procedures [11,12], showing enhanced perception accuracy, decreased completion times, and decreased peak and mean applied forces [12]. In TLM, given that the thickness of the laryngeal tissue is about 3~5mm [13], especially in the vocal cords, the regulation of tissue gripping forces is critical in ensuring that tissue trauma or rupture does not occur. The lack of gripping force feedback is also a limitation with He et al. [10]. Therefore, a suitable handling interface for any robot-assisted tool, which can reproduce the haptic sensation, is desirable.

## **1.2 Contributions**

With the objective of improving the surgeon-machine interface for instrument handling in TLM, the authors have explored prototype designs for robotic micro-forceps. A first prototype was presented in [14] which was a bulky design and unusable under the TLM microscope. A second version with a 1-DOF end-effector was presented in [15], with teleoperation control allowing precise motion, gesture scaling, and elimination of hand tremors and wrist excursions. This article presents the design of an updated version of the robotic micro-forceps device, having:

- (i) a motorized 2-DOF micro-forceps end-effector, with gripper jaw open/close and tool-shaft rotation for enhanced reachability;
- (ii) teleoperation control similar to [15];
- (iii) tissue gripping force (TGF) capability with impedance-based feedback for improved tissue surface perception; and
- (iv) updated experimental evaluation including phantom tissue based test bed and preliminary validation with expert surgeons.

The 2-DOF device integrated with a commercial 6-DOF serial manipulator arm (UR5 [16]) and including a force sensor (ATI Nano17 [17]), forms the RMF-2F, i.e., robotic microsurgical forceps with 2-DOF end-effector and force sensing, as seen in Fig. 3. The device is configured to be a 5-DOF setup: 3-DOF Cartesian positioning at the surgical site combined with the 2-DOF motorized micro-forceps end-effector. The RMF-2F is controlled by a haptic master device under unilateral teleoperation through the Omega.7 haptic master interface [18]. The following sections discuss the design, analysis, and evaluation of the proposed device.

## **2. DESIGN OF THE MOTORIZED 2-DOF MICRO-FORCEPS END-EFFECTOR**

Figure 2 points to the key constraints and requirements for any redesign of intraoperative tools in TLM. Table 1 lists the key features, which were considered in the design of the motorized 2-DOF device. Features 1 and 2 are derived from the dimensional constraints of TLM. Any mechanism to be used below the microscope and in-line with the surgical line-of-sight, in parallel with the laser beam itself, would need to have a small thickness to avoid vision occlusion and interference with the laser. The values for these features are arrived at empirically through measurements of the traditional setup and instruments, and discussions with expert surgeons. Consequently, any actuators for the motorized DOFs would have to be placed away from the line-of-sight. The main components of the 2-DOF micro-forceps are: (i) the tool shaft, (ii) the tool shaft holder, and (iii) the tool actuation mechanism.

### **2.1 The Tool Shaft**

The tool shaft is adapted from the traditional micro-forceps themselves. The traditional tool shaft has an outer shaft diameter of  $\phi = 2\text{mm}$  with an inner translating wire (itw,  $\phi = 1\text{mm}$ ). The translation of this wire (by 3mm, determined experimentally) provides the open-close DOF for the tool jaws. To adapt this traditional tool, the proximal end of the tool shaft is modified by attaching a hollow extension tube with external M3 threading to it. This modification is termed as the docking interface (DI) (Refer Fig. 4). The itw passes through the hollow DI to attach to the tool actuation mechanism, while the outer shaft attaches to the tool shaft holder.

### **2.2 The Tool Shaft Holder**

Figure 5 shows the design of the tool shaft holder, which supports the tool shaft as well as the tool actuation mechanism. It comprises of three sub-frames: F1, F2, and F3. A housing mounted on F1,  $H_S$ , supports the tool shaft via DI at point P1.  $H_S$  houses two small ball bearings  $B_f$  and  $B_r$ . The DI is held within the bearings

to incorporate the rotational DOF of the tool shaft. For the open/close DOF, the itw is extended just beyond  $H_S$  at point P1 to attach properly to the tool actuation mechanism. The cross-sectional thickness of  $H_S$  is designed to be 8mm, to limit its thickness and therefore the occlusion under the microscope. Further, the sub-frames F1 and F2 are rigidly connected at P2. The sub-frame F3 supports the linear actuator driving the open/close DOF of the tool shaft jaw while F2 supports the rotary motor providing the rotational DOF. The locations and dimensions for the components shall become clear in the following subsections.

## 2.3 The Tool Actuation Mechanism

### 2.3.1 Open/Close DOF

The mechanism consists of five linkages (L1, L2, L3, L4, L5), as referred in Fig. 6, designed to provide linear translation of the itw. Link L1 is considered as ground, i.e., the hinge link. Link L2 forms the input link along the actuator axis and it transfers direct motion to link L3, which in-turn transfer's inverse motion to link L4 about L1. L4 is directly coupled to L5 and the driven link L5 is attached to the itw.

The Nanotec L2018 linear actuator, with 30 N feed force, is chosen to drive the Open/Close DOF. It is placed on sub-frame F3 and is attached to the mechanism through L2. The force sensor is located at L2 with its measurement axis coincident with the actuator axis. The closing of the forceps jaws on the tissue produces a reaction force in the itw and thereby on the surface of the sensor through the five linkages. The force sensor outputs a signal in direct proportion to the gripping action<sup>1</sup>.

The five-linkage mechanism needs to be suitably dimensioned to ensure straight-line motion of the itw. This was done using the graphical synthesis method and the Function Generator technique [19] (Refer Fig. 6).

- (i) In stage-1, the lower three-link part is designed to be actuated by link L2 (i.e., F-E). The kinematic synthesis [20] begins with an arbitrary choice of the actuator axis and a point A at an offset of 50mm in the Y-direction from it. Point A is grounded through the ground link L1, and defines the support axis passing through it and parallel to the actuator axis. On the support axis, another point C is chosen at a distance of 10mm from point A in the X-direction. The intersection of the perpendicular dropped from point A and the actuator axis becomes point E. A suitable length in the X-direction from point E on the actuator axis gives point F, forming link L2, i.e., F-E. Then, joining the points A-C-E forms the triangular link L3. The linear displacement of link L2 (between points  $x_i$  (initial) and  $x_f$  (final)) causes

---

<sup>1</sup> Only the Z-axis force component of the ATI Nano17 is used for measuring the TGF. Isolating the friction between moving links from the measured force value is part of future work and is ignored for the purposes of this paper.

link L3 to rotate about point A within angular limits  $\theta_i$  and  $\theta_f$ . To ensure a straight-line trajectory of L2 between  $x_i$  and  $x_f$ , the principle of Chebyshev precision points [18], as given by Eq. 1, is used.

$$x_j = a - h \cos \left[ (2j - 1) \cdot \frac{\pi}{2n} \right] \quad j = 1, 2, 3 \quad (1)$$

The variables 'a' and 'h' are defined as  $(x_i + x_f)/2$  and  $(x_f - x_i)/2$  respectively. Considering a small displacement, say 1mm, 'n' is chosen as 3. The link L2 starts from  $x_i$  (= 0mm), passes through the precision points  $x_1$ ,  $x_2$ ,  $x_3$ , and finishes its stroke at  $x_f$  (= 1mm) (Fig. 7(a)). The resulting three precision points are obtained as  $x_1 = 0.066\text{mm}$ ,  $x_2 = 0.5\text{mm}$  and  $x_3 = 0.933\text{mm}$ . Correspondingly, link L3 undergoes angular motion through  $(\theta_i, \theta_1, \theta_2, \theta_3, \theta_f)$  about point A. With such an arrangement though, due to the angular motion of link L3, its end-point E has a simultaneous displacement of 0.0130mm in the Y-direction (Refer Fig. 7(b)). A small cavity is introduced in link L3 at end-point E to accommodate this displacement and ensure that link L2 translates in X-direction only.

- (ii) In the second stage, a hinge point D is chosen along the support axis at a further distance of 10mm from point C in the X-direction. Another point B is then assumed at a distance of 150mm from the support axis in the Y-direction. The triangular link B–C–D so created forms link L4. The axis passing through B and parallel to the support axis becomes the tool shaft axis. Point C serves as the common engagement point for links L3 and L4. This implies that the angular motion of link L3 is mirrored by link L4 at point C. The key insight here is the choice of the distances for points A and B. As stated in Table 1, the optimal displacement between the tool-base and the microscope line-of-sight is 200mm. Here, through the choices of 50mm and 150mm for points A and B, the total distance between the tool shaft axis and the actuator axis becomes 200mm. Additionally, the link-length ratio for L4:L3 becomes 3:1. Thus, a 1mm displacement of point E results in a 3mm displacement of end-point B (Refer Fig. 7(c)). Here again, a cavity is provided in L4 at point B to accommodate its Y-displacement of 0.0075mm due to its angular motion (Fig. 7(d)). The angular motion of link L4 is transferred to L5 (B–G) such that it produces the corresponding straight-line translation of the attached itw resulting in the open/close of the micro-forceps jaws.

Finally, the synthesized mechanism is analysed for its mobility DOFs using the Grübler's criterion [21]. The mechanism has two mobility DOFs: the first DOF is the linear translation of link L5 and the second DOF is the negligible motion for the end-point B in the Y-direction.

### 2.3.2 Rotational DOF

The mechanism for the rotational DOF is implemented as the coordinated motion of three components:

(i) Miter Gear assembly (MG); (ii) Spur gear assembly (SG); and (iii) Modified link L5 mechanism ( $M_{L5}$ ) (Refer Fig. 8).

- (i) **Miter Gear assembly, (MG):** The tool shaft rotation is made possible through a miter-gear assembly with an outer diameter<sup>2</sup> of 8mm, in compliance with the TLM constraints of Table 1 (Refer Fig. 8(a)). The orthogonal gear  $G_O$  is mounted onto a shaft  $S_O$  such that it is orthogonal to the tool shaft axis. The axial gear  $G_A$  is mounted co-axial with the tool shaft axis and attached rigidly to the DI of the tool shaft. Any rotation on the miter-gear assembly  $G_O$ -to- $G_A$  is transferred to the tool shaft through DI.
- (ii) **Spur Gear assembly, (SG):** The rotation of shaft  $S_O$  is obtained through a low-backlash 1:1 spur-gear assembly ( $SG_1$  and  $SG_2$ ) (Refer Fig. 8(b)). This assembly transfers the rotary motion of the actuator ( $R_M$ , Nanotec SC2018 with 1.8 N-cm torque) to  $S_O$ , and in-turn to  $G_O$ -to- $G_A$ . An additional ball bearing ( $B_b$ ) supports the rotation of  $S_O$  and reduces the vibration in the rotary motion.
- (iii) **Modified link L5 in the open/close DOF, ( $M_{L5}$ ):** To allow simultaneous rotation and translation of the itw (through the DI), a suitable adaptation is necessary in link L5. Three components are introduced for this purpose: (i) a specially designed holder ( $H_I$ ) with set-screws to attach the itw. The holder includes a small shaft extension; (ii) this small shaft is inserted into a small ball-bearing ( $B_S$ ), thereby allowing  $H_I$  to rotate freely; (iii)  $B_S$  is held within a housing  $H_B$  which is integrated with link L4 (Fig. 8(c)).

With these adaptations, the motorized micro-forceps has 2-DOFs and complies with the TLM constraints.

## 3. INTEGRATION OF THE ROBOTIC MICRO-FORCEPS – RMF-2F

As seen in Fig. 3, the 2-DOF motorized micro-forceps tool is attached as an end-effector to the UR5 robotic manipulator at a 90° angle, resulting in the RMF-2F device. The UR5, seen in Fig. 9(a), has a payload capacity of 5 kg, repeatability of 0.1mm, a reach radius of 850mm, and can be controlled at 125 Hz. These values make it suitable for precise teleoperation control. Since the motorized micro-forceps already has a rotational DOF, the final orientation DOF of the UR5 is not used. The D-H parameters of the integrated RMF-2F device are suitably updated as a 5-DOF global device (3-DOF positioning + 1 DOF rotation + 1 DOF open/close), as given

---

<sup>2</sup> This is within the  $H_S$  thickness of 8mm.

in Table 2 and Fig. 10. Here,  $l_6$  and  $l_7$  refer to the dimensions of the motorized 2-DOF micro-forceps. In this case,  $l_6 = 210\text{mm}$  and  $l_7 = 200\text{mm}$ .  $q_{rot}$  is the rotation angle of the rotary DOF.

#### 4. TELEOPERATION CONTROL AND VALIDATION

A master haptic interface, the Force Dimension Omega.7, as seen in Fig. 9(c), teleoperates the RMF-2F. The Omega.7 has 7-DOFs (6-DOF motion + 1-DOF gripper), of which the three translational DOFs and the gripper DOF are active, while the rotational degrees of freedom are passive. The gripper DOF commands the open/close of the forceps jaws for tissue gripping; the measured TGF is also rendered to the same DOF. The three translational DOFs control the 3-DOF positioning of the RMF-2F, as explained in Sec. 3. The Omega.7 provides features like active gravity compensation to improve the teleoperation transparency and reduce the operator's fatigue, which are desirable features in surgical applications. The integrated system uses a dedicated Gigabit Ethernet connection between the master and RMF-2F device, ensuring minimal time delay between the two. A time-domain, two-layer controller [22] preserves the stability and transparency of the system, ensuring safe teleoperation.

- (i) It is evident that the kinematics of this master interface and the RMF-2F device are non-homothetic. To overcome this limitation, instead of a position-based controller, a velocity-based teleoperation controller is implemented, where the end-effector velocity of the master is commanded to the end-effector (i.e., micro-forceps tool-tip) velocity of the RMF-2F. This was possible within the requirements of the narrow workspace for the micro-forceps, inside the laryngoscope. The 3-DOF master end-effector velocity ( $\dot{q}_h \in \mathbb{R}^3$ ) is filtered and scaled with a gesture scaling factor  $\zeta$  and mapped to the velocity ( $\dot{q}_r \in \mathbb{R}^3$ ) of the RMF-2F, as shown in Eq. 2. The constants have values:  $\zeta = 0.2$  and  $\beta = 0.025$ , adapted from [14].

$$\begin{aligned} \dot{q}_h^k &= (1 - \beta) \cdot \dot{q}_h^{k-1} + \beta \cdot \dot{q}_h \\ \dot{q}_r^k &= J^{-1} \cdot \dot{q}_h^k \cdot \zeta \end{aligned} \quad (2)$$

$J^{-1}$  is the inverse of the manipulator Jacobian matrix,  $J \in \mathbb{R}^{3 \times 3}$ . With the above scaling, the integrated system was tested by moving the master in free-space over a period of 120 seconds, and recording the corresponding position of the RMF-2F. Figure 11 shows the plot for the motion in one axis for the trial, including the tracking error. The root mean square error in the 3-axis positioning for RMF-2F was found to be 0.3901mm with a standard deviation of 0.3829mm. The position mapping error is therefore less than 400 $\mu\text{m}$ , indicating transparency and accuracy.

(ii) For the control of the motorized 2-DOF micro-forceps end-effector, unlike the above scheme, unilateral position control is implemented; the yaw and gripper DOFs of the master device command the rotation and open/close DOFs of the RMF-2F respectively. The relationship is shown by Eq. 3, where  $\eta_1 = 3$  and  $\eta_2 = 2$  are empirically chosen to compensate for the friction and hysteresis in the system. The control loop was run at 100Hz.

$$\begin{bmatrix} q_{rot} \\ q_{jaw} \end{bmatrix} = \begin{bmatrix} \eta_1 & 0 \\ 0 & \eta_2 \end{bmatrix} \begin{bmatrix} q_h^{yaw} \\ q_h^{grip} \end{bmatrix} \quad (3)$$

(iii) For force sensing, the ATI Nano17 Force/Torque sensor (Fig. 9(b),  $\phi = 17\text{mm}$ ,  $L = 14.5\text{mm}$ ), offers a fine resolution of 3.125 mN with sensing up to 70 N, and registering data at 7 kHz. The TGF at the sensor was independently evaluated through a customized mechanism, replicating the arrangement seen in Fig. 5. As seen in Fig. 12(a), a high-precision X-Y table (Siskiyou 1620-XYZR [23]) controls the open/close of the micro-forceps. For different internal angles of the jaws, the sensor output signal was recorded while gripping ex-vivo chicken tissue samples (min.  $40 \times 40\text{mm}^2$  area and 5mm thickness). For every angle, the sensor values were averaged over 5 trials with 5 different tissue samples. As seen from Fig. 12(b), the value increases non-linearly from the fully-open position of the micro-forceps ( $90^\circ$ , tissue not touching the jaws) to the fully-closed position (around  $0^\circ$ ). These values are in-line with those seen in [24].

## 5. EXPERIMENTAL EVALUATION

The performance of the RMF-2F device was validated through evaluation experiments simulating real surgical actions like grasping, pulling, and manipulating the laryngeal tissue. These trials were performed with 10 non-medical subjects (Mean age = 28.2 years; 8 Males, 2 Females) with no prior experience in such tasks. They subjects operated the Omega.7 to command the RMF-2F for pick-rotate-n-place tasks, as seen in Fig. 13. A test bed with different shaped objects (triangle, rectangle, semi-circle, and circular ring) placed in cavities was prepared, as seen in Fig. 13(b) and (c). The top surface of these shapes was provided with a phantom tissue-like material to allow the sensation of tissue gripping. The phantom tissue is a bi-component polyurethane elastomer (F-105 A/B 5 shore, from BJB Enterprise) added with a softening agent (SC- 22, from BJB Enterprise) [25]. For uniformity of results, each trial began with the RMF-2F in home position (15mm above the test bed). The experiments were conducted in two conditions, C1 (haptic feedback activated) vs C2 (haptic feedback deactivated).

In condition C1, the measured TGF is rendered to master interface gripper (7<sup>th</sup>) DOF itself. To do this, the force sensor value was first filtered using a low-pass filter ( $\beta = 0.001$ , Eq. 4), to suppress noisy signals. It is then scaled based on the internal angle of the micro-forceps jaws using Eq. 5. This value becomes a scaling factor for the feedback to the gripper DOF using Eq. 6. Here,  $\Omega_g$  is the maximum internal angle of the jaws in open position, i.e.,  $90^\circ$  and  $\omega_g^k$  is the internal angle at instant k. After extensive offline testing, the values of the constants were obtained as  $c = 1.5$  and  $\gamma = 1/20$ , giving  $1.5 < k^k < 5.5$ . The rendered force therefore varies in proportion to the sensed force as well as the internal angle of the gripping jaws, giving an impedance-based haptic feedback.

$$f_g^k = (1 - \beta) \cdot f_g^{k-1} + \beta \cdot f_g^{sensor} \quad (4)$$

$$k^k = \gamma \cdot (\Omega_g - \omega_g^k) + c \quad (5)$$

$$f_g^{omega} = \begin{cases} 0, & f_g^k \leq 0 \\ k^k \cdot f_g^k, & f_g^k > 0 \end{cases} \quad (6)$$

Before each subject, the mechanism is calibrated to ensure that open/close of micro-forceps jaws in free space outputs a non-positive signal for  $f_g^{sensor}$ , which is suppressed. Figure 14 shows the behaviour of Eq. 6 for the  $\omega_g^k$ ,  $f_g^k$ , and  $f_g^{omega}$  for a sample trial with the Triangle shape. As is seen,  $f_g^k$  varies between -1 and 2 N, while  $f_g^{omega}$  varies between 0–10 N, through the various phases of: closed jaws ( $0^\circ$  angle), micro-forceps opening ('A'), shape gripped ('B'), shape release initiated ('C'), and shape released ('D').

Subjects conducted 8 trials each (twice on each shape) in the following order: (i) Semi-circle, (ii) Ring, (iii) Triangle, and (iv) Rectangle. The conditions C1 and C2 were randomized across the trials for obtaining unbiased evaluation. The device performance was analysed by measuring the: (i) Trajectory followed by the RMF-2F for the tasks; (ii) Execution time required to conduct the tasks; (iii) Number of failed attempts during task execution; and (iv) TGF feedback performance in C1 and C2 conditions.

## 5.1 Trajectory Analysis

Figure 15(a) shows a sample trajectory for the RMF-2F with the Triangle shape, starting from the home position, picking-up the object from its cavity, and then placing it in the other cavity. As the subjects were required to re-orient the objects after picking up, the quantified angular rotation ( $180^\circ$  in case of the Triangle) for the trial is shown in Fig. 15(b), where the radial direction represents the time in seconds. For analysing the usability of the device, the trajectory ratio was used as a metric. With 8 consecutive trials, the trajectory length for the first trial was used as the basis against which the ratios for the 7 succeeding trials were calculated. Figure 16(a) shows the overall trend of the ratios over time indicating that the subjects find the device easy and quick to learn. The ratio

of the 8<sup>th</sup>-to-first trial is 0.6988, while the average ratio over the 7 trials is 0.9111. The positive performance for the device is attributed to the ease-of-learning offered by the Omega.7 interface and its transparent integration with the RMF-2F.

## 5.2 Execution Time and Controllability

A similar downward trend in the time taken for the task completion demonstrates the RMF-2F's ease-of-learn-ability. Figure 16(b) shows such trends for the two metrics: (i) time to lift the shape from the cavity ( $T_{\text{lift}}$ ); and (ii) time to transfer the shape ( $T_{\text{total}}$ ). As observed,  $T_{\text{lift}}$  goes from 43.2s to 28.8s, an improvement of 33.3%. The same trend is seen for  $T_{\text{total}}$ , going from 84.2s to 49.9s, giving an improvement of almost 40%.

In terms of controllability, over all the trials (a total of 80), only 18 failed attempts (failure to lift the shape or transfer it to the other cavity) were recorded in task execution.

## 5.3 Tissue Gripping Force analysis

TGF feedback analysis was conducted using the  $f_g^k$  value from Eq. 6. Figure 17(a) shows a sample trial for the Triangle shape in the C1 and C2 conditions, where the difference in levels of force is evident. The highlighted locations indicate phases of the task. An overall comparison of the average values of TGF for all the subjects showed that the average force applied on phantom tissue is less in condition C1 (1.624 N) in comparison to C2 (2.116 N), as seen in Fig. 17(b). This difference is statistically significant according to the *Student's t-test* ( $p = 0.0486$ ). Similarly, the value for the maximum TGF is less in C1 (5.532 N) than in C2 (6.768 N), although not statistically significant ( $p > 0.05$ ). For soft tissue, the closing of the micro-forceps jaws causes the tissue to be displaced around the jaws, thereby causing a non-linear variance (and reduction) in the gripping force. By incorporating the internal jaw angle in the force feedback, this effect of squeezing soft tissue can be compensated for, providing a more natural tissue gripping sensation. This results in better regulation of gripping forces in the C1 condition, where the subjects applied less force on the phantom tissue, as compared to the C2 condition. C1 condition allows better tissue surface perception and improved safety against potential tissue trauma.

Furthermore, in terms of controllability, out of the 18 failed trials recorded, 8 were in the C1 condition as against 10 in the C2 condition, which does not conclusively distinguish the two conditions.

## 6. DISCUSSIONS

The final aim is the introduction of RMF-2F in the TLM operating room (OR) and therefore it is important to know if the improved functionality of the device and the TGF feedback feature is useful for the real end users, i.e., the surgeons. In this regard, three surgeons from the San Martino Hospital in Genoa (Italy) were invited to perform preliminary experiments using the RMF-2F device. Ex-vivo pig larynxes to closely simulate the human larynx and the surgical setup was replicated similar to the OR, including the surgical microscope, laryngoscope, and laser micro-manipulator, as seen in Fig. 18. The surgeons were asked to perform grasping, pulling, turning, and manipulating of the tissue. The surgeons provided very useful informal feedback as follows:

- (i) **Appreciation of tool rotation:** The tool-tip rotation functionality was appreciated by the surgeons. It helped them to easily reach different areas of the vocal region. Also, they were able to grip-n-turn the tissue in order to have clearer vision of the underlying tissue.
- (ii) **Appreciation of TGF feedback:** While using the device under two different feedback conditions (C1 and C2), surgeons could distinguish between gripping action on tissues, and regulate forces applied on the tissue. The value of the gripping forces was not measured in these trials due to limited number of subjects.
- (iii) **Vision occlusion under microscope:** As discussed in Table 1, the device was designed in order to avoid vision occlusion under the microscope. Nevertheless, the surgeons complained about partial vision occlusion. Although this implies the need to further reduce the device dimensions, it also indicates a requirement of training on the part of the surgeons to control the robotic device through teleoperation. Surgeons easily use similarly thick traditional tools manually under the microscope, which is a result of years of training for hand-eye coordination with the tools.

## 7. CONCLUSIONS

This paper presented a novel design of a 5-DOF robotic microsurgical forceps device for intraoperative use in TLM, integrated with a teleoperation haptic master, Omega.7, and the ATI Nano17 force sensor. The RMF-2F device is compliant with the constraints of TLM, and offered: (i) enhanced tool reachability through motorized tool-tip rotation; (ii) greater precision in motion, stable positioning, no hand tremors, reduced wrist excursions, and gesture scaling through teleoperation; and (iii) improved controllability and safety through an ergonomic teleoperation master along with improved tissue gripping haptic feedback. The experimental analysis with different subjects quantified and validated the above-mentioned features. Preliminary trials with surgeons indicated appreciation for the design and functionalities offered by the device.

In future works, along with improvements in device form-factor, the gripping force shall be further investigated for isolating different components like stretching, twisting, etc. At this stage, the force sensor value is low-pass filtered to suppress the noise from the moving mechanisms in the system. Therefore, the limits of stability and transparency of the robotic teleoperation shall be established for intuitive behaviour.

## **ACKNOWLEDGEMENTS**

The authors would like to thank the clinical staff and research team of the ENT unit at the San Martino Hospital: Prof. Giorgio Peretti, Dr. Francesco Mora, and Dr. Luca Guastini for their expert inputs and support during the device development.

## **REFERENCES**

1. Jako GJ (1972) Laser surgery of the vocal cords: an experimental study with carbon-dioxide lasers on dogs. *The Laryngoscope* 82 (12):2204-2216.
2. Liverneaux PA, Berner SH, Bednar MS, Parekattil SJ, Ruggiero GM, Selber JC (2012) *Telemicrosurgery: robot assisted microsurgery*. Springer-Verlag, Paris.
3. Hirano M (1974) Morphological structure of the vocal cord as a vibrator and its variations. *Folia Phoniatica et Logopaedica* 26 (2):89-94.
4. Da Vinci Surgical System (2018) *Intuitive Surgical*. [www.intuitivesurgical.com](http://www.intuitivesurgical.com). Accessed on 30<sup>th</sup> March 2018.
5. Simaan N, Taylor R, Flint P (2004) A dexterous system for laryngeal surgery. In: *Proceedings of IEEE International Conference on Robotics and Automation, IEEE*, pp 351-357.
6. Wang S, Li Q, Ding J, Zhang Z (2006) Kinematic design for robot-assisted laryngeal surgery systems. In: *Proceedings of IEEE/RSJ International Conference on Intelligent Robots and Systems, IEEE*, pp 2864-2869.
7. Rivera-Serrano CM, Johnson P, Zubiato B, Kuenzler R, Choset H, Zenati M, Tully S, Duvvuri U (2012) A transoral highly flexible robot. *The Laryngoscope* 122 (5):1067-1071.
8. Solares CA, Strome M (2007) Transoral robot-assisted co2 laser supraglottic laryngectomy: Experimental and clinical data. *The Laryngoscope* 117 (5):817-820.
9. Desai SC, Sung CK, Jang DW, Genden EM (2008) Transoral robotic surgery using a carbon dioxide flexible laser for tumors of the upper aerodigestive tract. *The Laryngoscope* 118 (12):2187-2189.

10. He C, Olds K, Iordachita I, Taylor R (2013) A new ENT microsurgery robot: error analysis and implementation. In: Proceedings of IEEE International Conference on Robotics and Automation, IEEE, pp 1221-1227.
11. Okamura AM (2004) Methods for haptic feedback in teleoperated robot-assisted surgery. *Industrial Robot* 31 (6):499-508.
12. Van der Meijden O, Schijven M (2009) The value of haptic feedback in conventional and robot-assisted minimal invasive surgery and virtual reality training: a current review. *Surgical Endoscopy* 23 (6):1180-1190.
13. Wong BJ, Jackson RP, Guo S, Ridgway JM, Mahmood U, Su J, Shibuya TY, Crumley RL, Gu M, Armstrong WB (2005) In vivo optical coherence tomography of the human larynx: normative and benign pathology in 82 patients. *The Laryngoscope* 115 (11):1904-1911.
14. Deshpande N, Chauhan M, Pacchierotti C, Prattichizzo D, Caldwell DG, Mattos LS (2016) Robot-assisted microsurgical forceps with haptic feedback for transoral laser microsurgery. In: Proceedings of IEEE International Conference of the Engineering in Medicine and Biology Society, 38<sup>th</sup> edn., IEEE, pp 5156-5159.
15. Chauhan M, Deshpande N, Barresi G, Pacchierotti C, Prattichizzo D, Caldwell DG, Mattos LS (2017) Design and control of a novel robotic microsurgical forceps for Transoral Laser Microsurgery. In: Proceedings of IEEE International Conference on Advanced Intelligent Mechatronics, IEEE, pp 737-742.
16. UR5 manipulator (2018) Universal Robot. [www.universal-robots.com/products/ur5-robot](http://www.universal-robots.com/products/ur5-robot). Accessed on 30<sup>th</sup> March 2018.
17. Nano17 Force Sensor (2018) ATI. [www.ati-ia.com/Products/ft/ft\\_models.aspx?id=Nano17](http://www.ati-ia.com/Products/ft/ft_models.aspx?id=Nano17). Accessed on 30<sup>th</sup> March 2018.
18. Omega.7 (2018) Force Dimension. [www.forcedimension.com/products/omega-7/overview](http://www.forcedimension.com/products/omega-7/overview). Accessed on 30<sup>th</sup> March 2018.
19. Kinzel EC, Schmiedeler JP, Pennock GR (2007) Function generation with finitely separated precision points using geometric constraint programming. *Journal of Mechanical Design* 129 (11):1185-1190.
20. Suh CH, Radcliffe CW (1978) Kinematics and mechanisms design. Wiley, New York.
21. Gogu G (2005) Chebyshev–Grübler–Kutzbach's criterion for mobility calculation of multi-loop mechanisms revisited via theory of linear transformations. *European Journal of Mechanics-A/Solids* 24 (3):427-441.
22. Franken M, Stramigioli S, Misra S, Secchi C, Macchelli A (2011) Bilateral telemanipulation with time delays: A two-layer approach combining passivity and transparency. *IEEE Transactions on Robotics* 27 (4):741-756.

23. 1620-XYZR Motion Table (2018) Siskiyou. [http://www.siskiyou.com/ProductDetail/14970000e\\_1620xyzr](http://www.siskiyou.com/ProductDetail/14970000e_1620xyzr). Accessed on 30<sup>th</sup> March 2018.
24. Yamanaka H, Makiyama K, Osaka K, Nagasaka M, Ogata M, Yamada T, Kubota Y (2015) Measurement of the physical properties during laparoscopic surgery performed on pigs by using forceps with pressure sensors. *Advances in Urology* 2015:1-10. <http://dx.doi.org/10.1155/2015/495308>.
25. Ciullo A, Penza V, Mattos L, De Momi E (2016) Development of a surgical stereo endoscopic image dataset for validating 3D stereo reconstruction algorithms. In: *Proceedings of the Joint Workshop on New Technologies for Computer/Robot Assisted Surgery*, 6<sup>th</sup> edn., CRAS, pp 62-63.

## FIGURE CAPTIONS

**Fig.1** Traditional TLM surgical setup

**Fig.2** TLM dimensional constraints. (a) overall dimensions; (b) dimensions around the laryngoscope

**Fig.3** The 5-DOF “RMF-2F” device: 2-DOF micro-forceps end-effector integrated with the 6-DOF UR5 robot and the ATI Nano17 force sensor

**Fig.4** The tool shaft

**Fig.5** The tool shaft holder

**Fig.6** Kinematic synthesis of the open/close DOF of the tool actuation mechanism

**Fig.7** Curvi-linear motion of links L3 and L4. (a) Horizontal displacement for L3; (b) Vertical displacement for L3; (c) Horizontal displacement for L4; (d) Vertical displacement for L4

**Fig.8** Detailed view of the rotational DOF of the tool actuation mechanism. (a) Miter Gear Assembly, (MG); (b) Spur Gear Assembly, (SG); (c) Link L5 modification, ( $M_{L5}$ )

**Fig.9** Hardware components of the integrated RMF-2F setup. (a) UR5; (b) ATI Nano17; (c) Omega.7

**Fig.10** D-H parameters and kinematic structure of the 5-DOF RMF-2F

**Fig.11** Motion control evaluation of the RMF-2F

**Fig.12** Tissue gripping force sensing characterization. (a) Calibration setup; (b) Characterization plot

**Fig.13** Experimental evaluation setup. (a) Subject performing trial; (b) Test bed dimensions; (c) Test bed with phantom tissue shapes

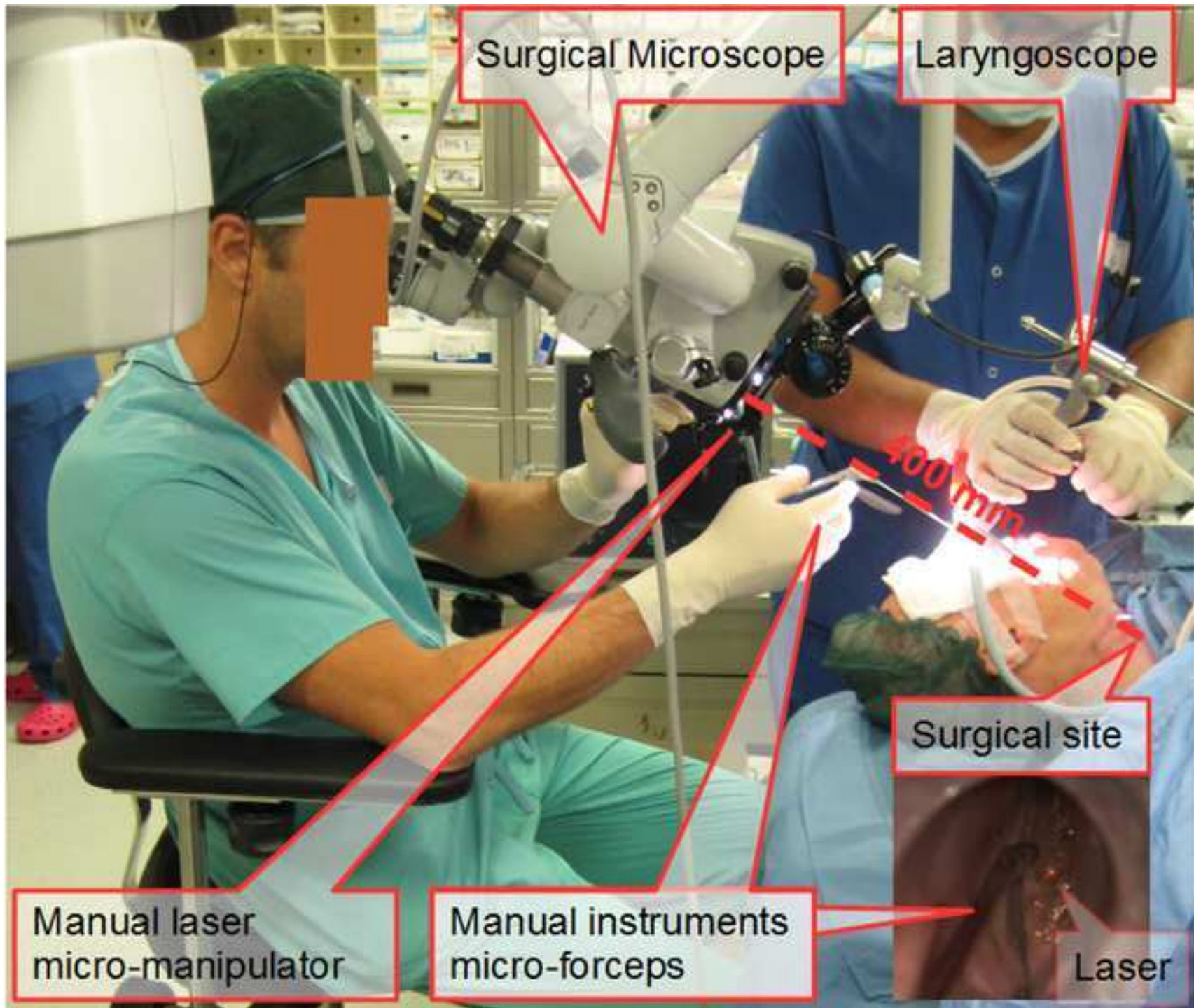
**Fig.14** Sample trial depicting behaviour of Eq. 6. The highlighted locations indicate the phases of the trial: ‘A’ = Micro-forceps opening; ‘B’ = Shape gripped; ‘C’ = Shape release initiated; ‘D’ = Shape release completed

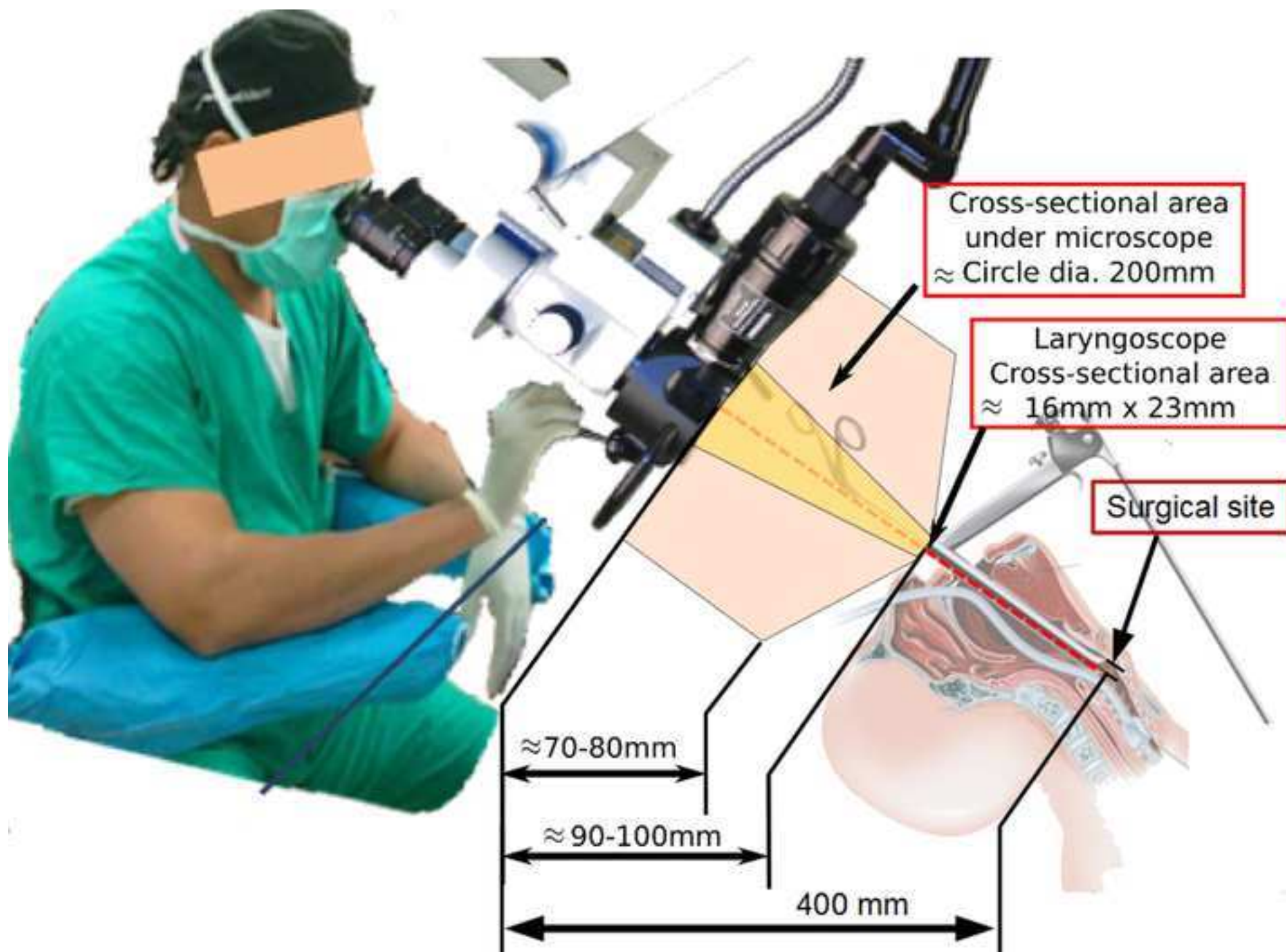
**Fig.15** RMF-2F trajectory during a sample trial. (a) 3-DOF position during task; (b) Angular orientation during task

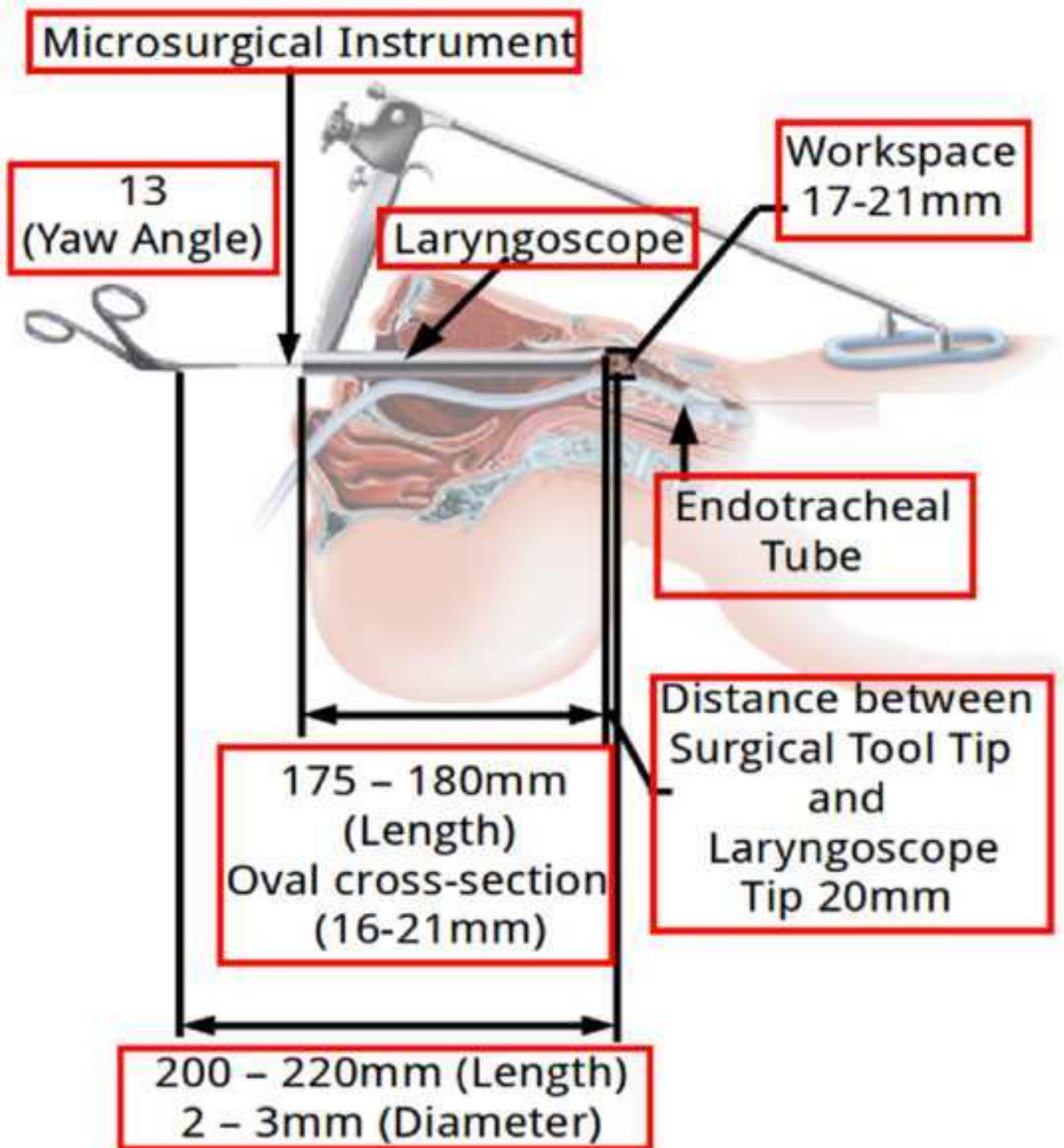
**Fig.16** Results of experimental evaluation. (a) Overall trajectory ratio; (d) Execution time

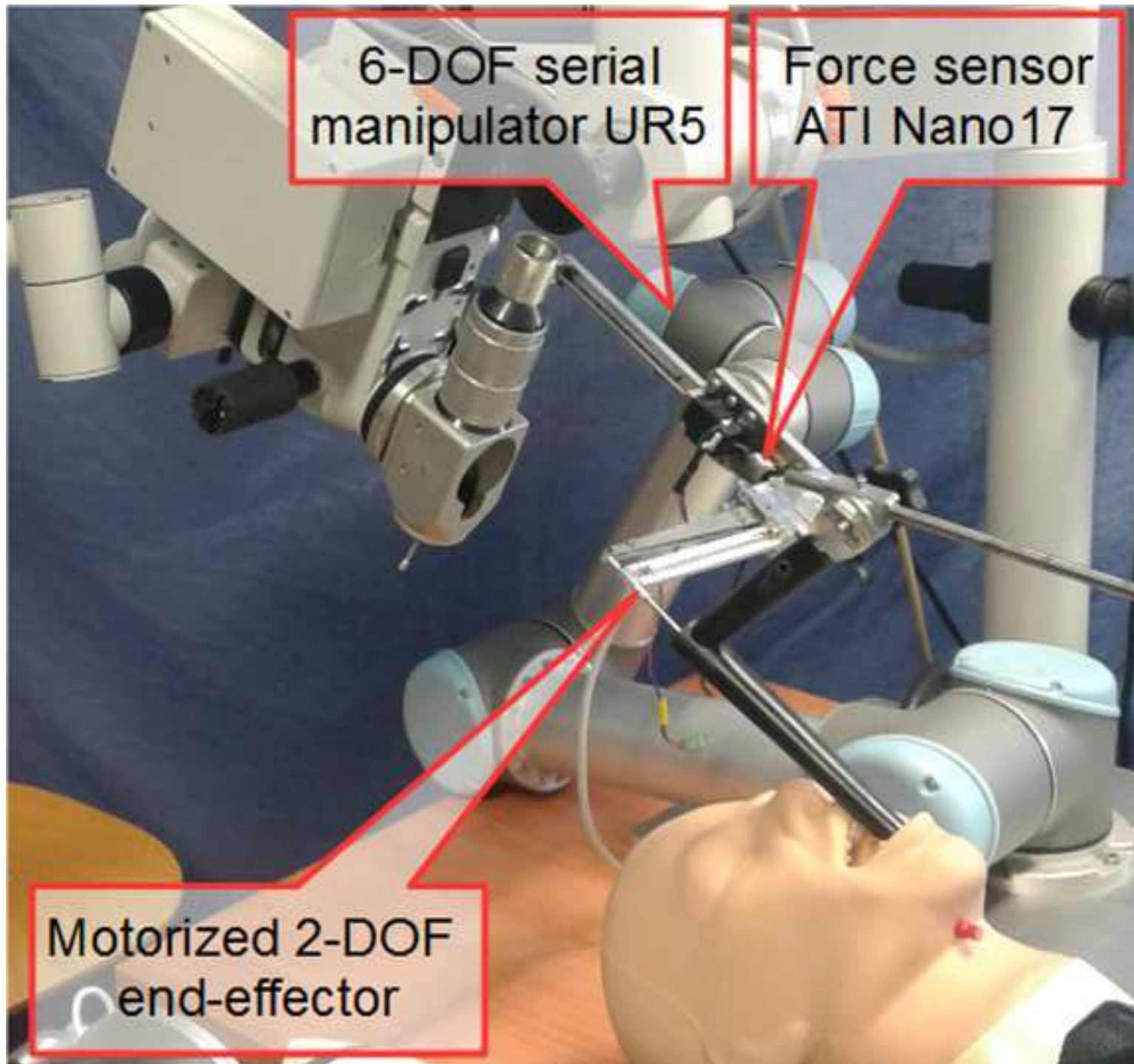
**Fig.17** Results of TGF analysis. (a) Difference in TGF values for C1 and C2 condition for a sample trial; (b) Comparison of mean and maximum TGF

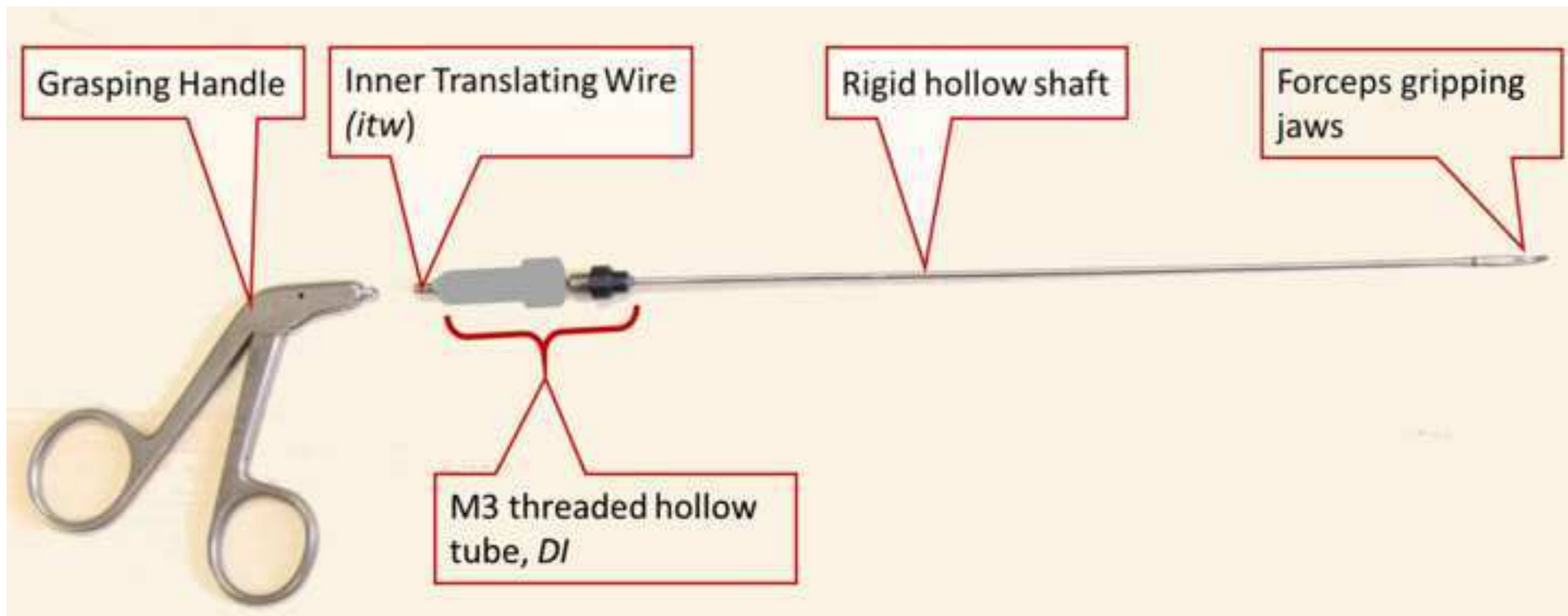
**Fig.18** Setup for preliminary trials of RMF-2F with expert surgeons

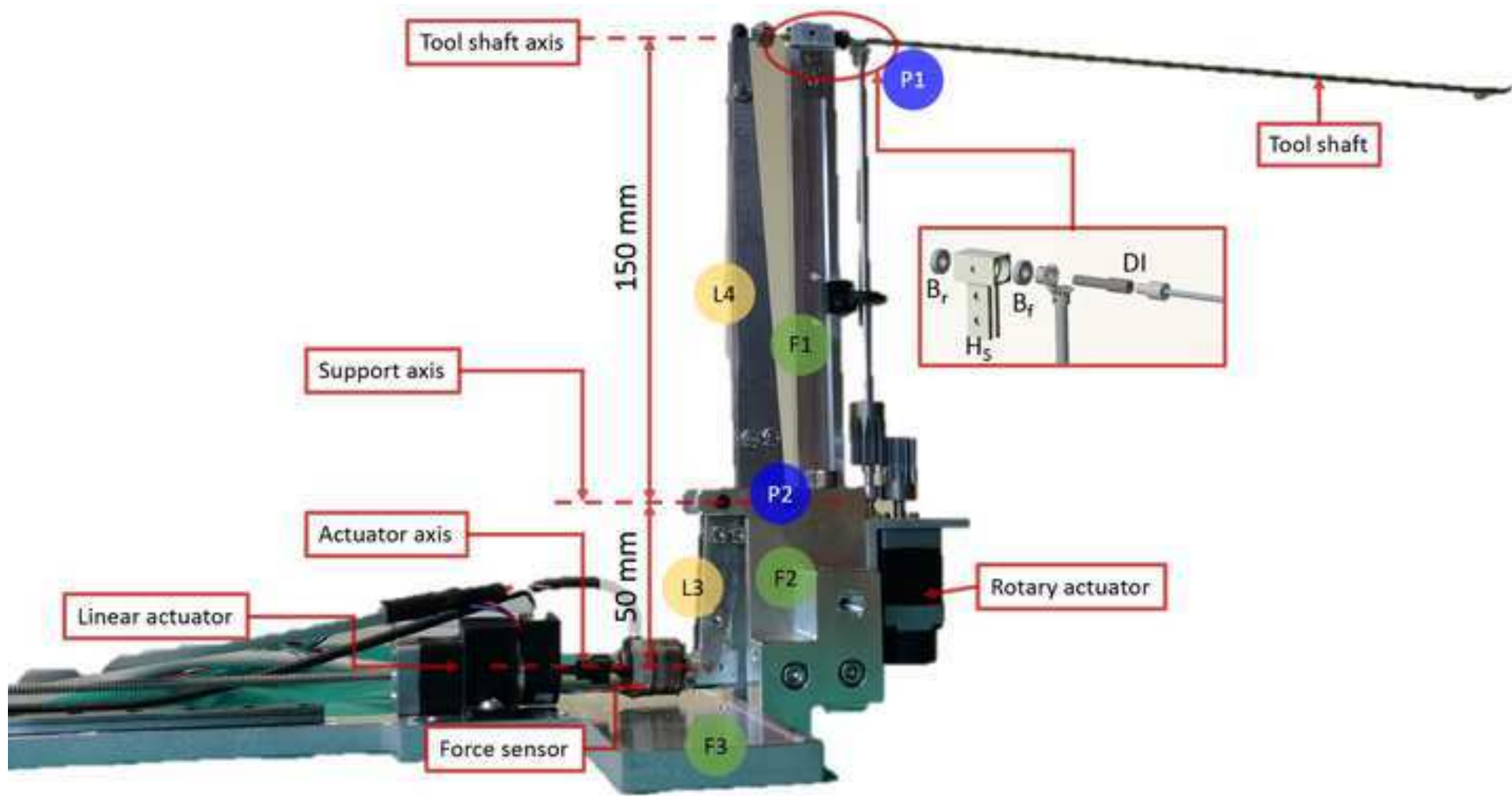












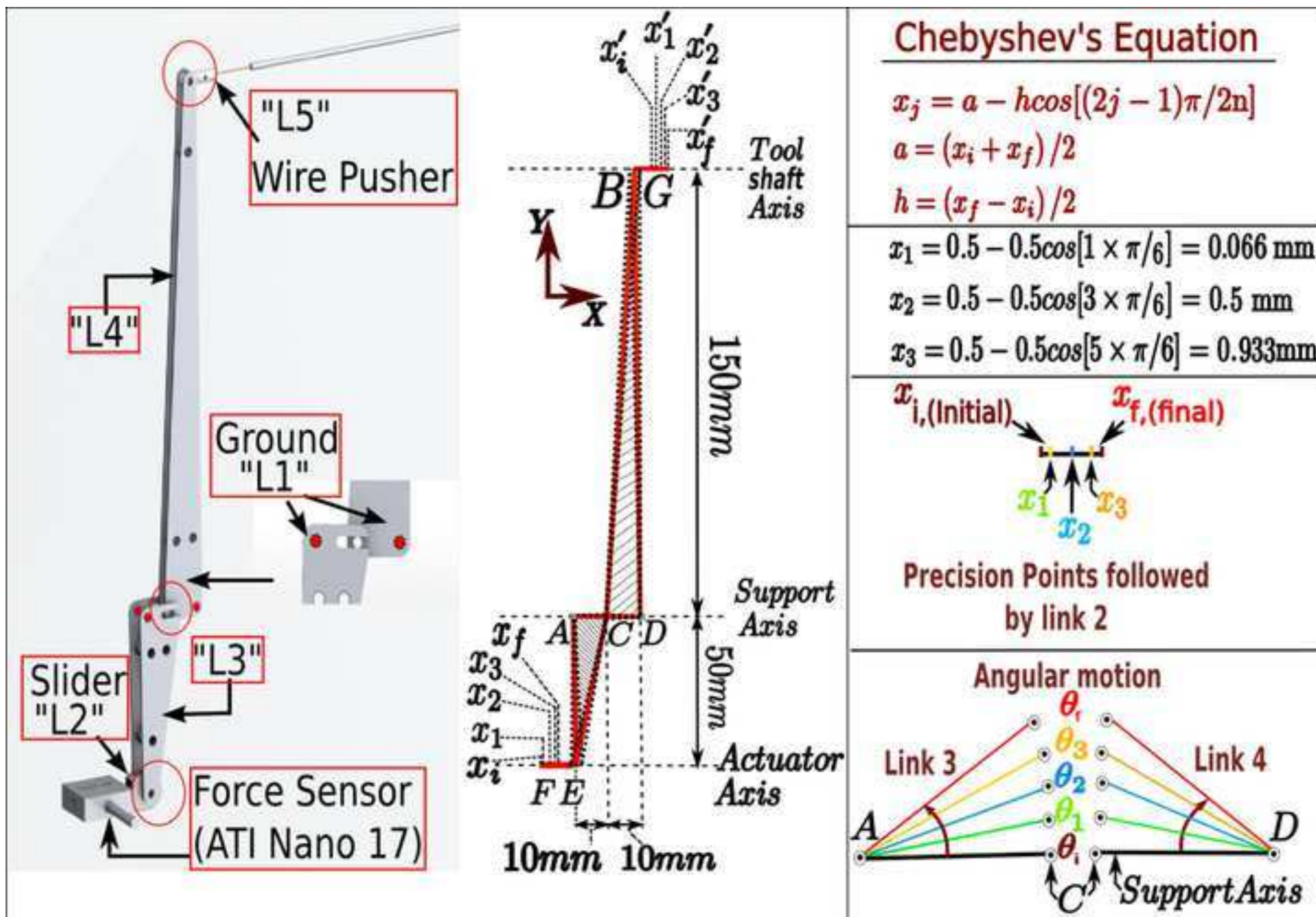
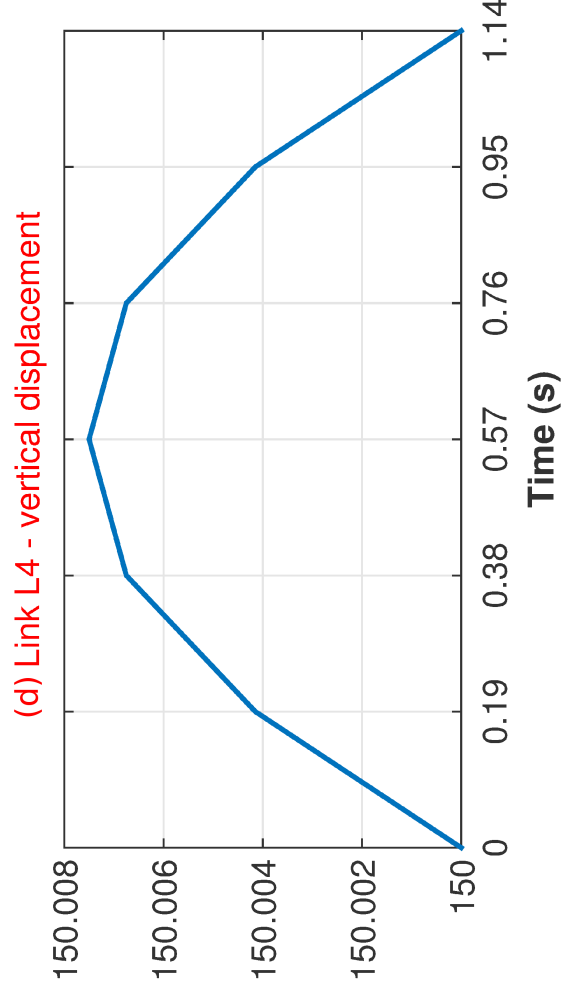
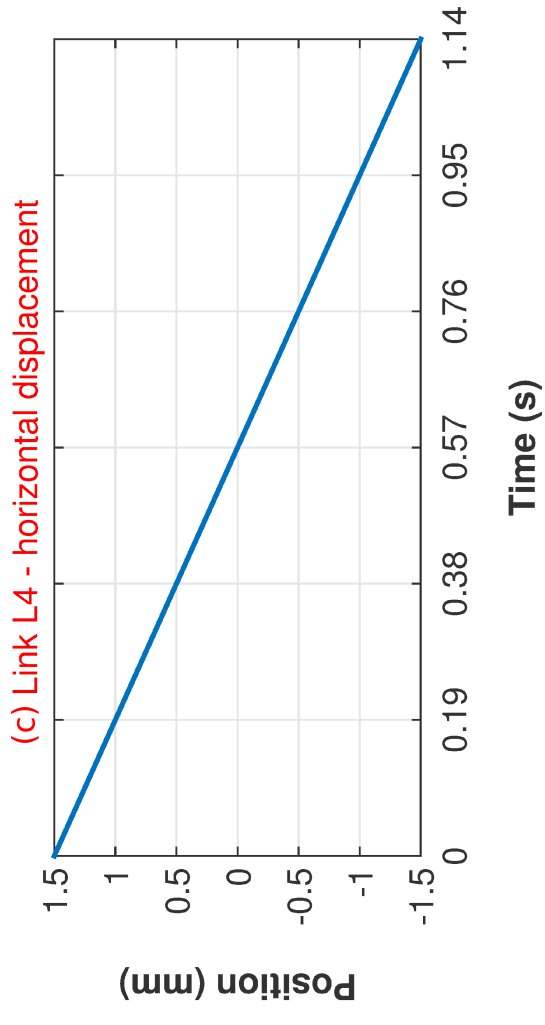
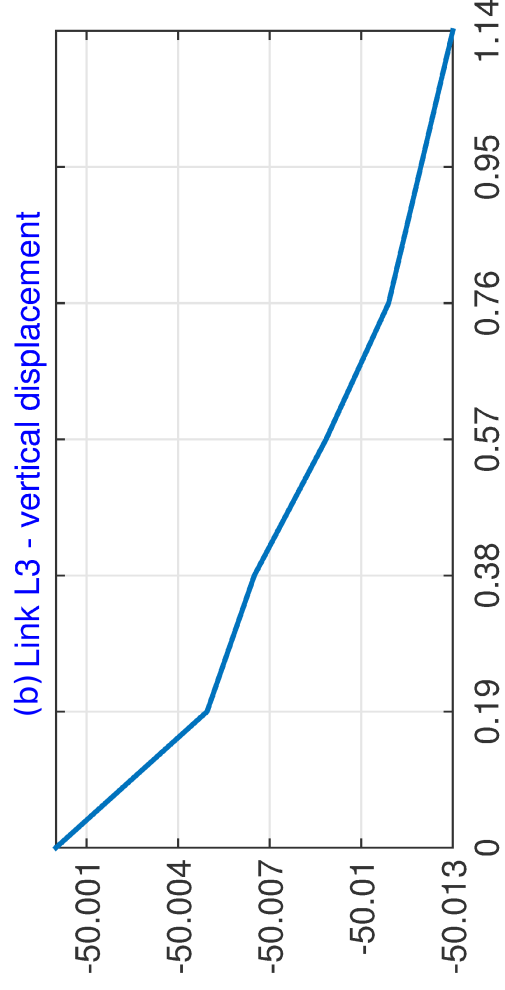
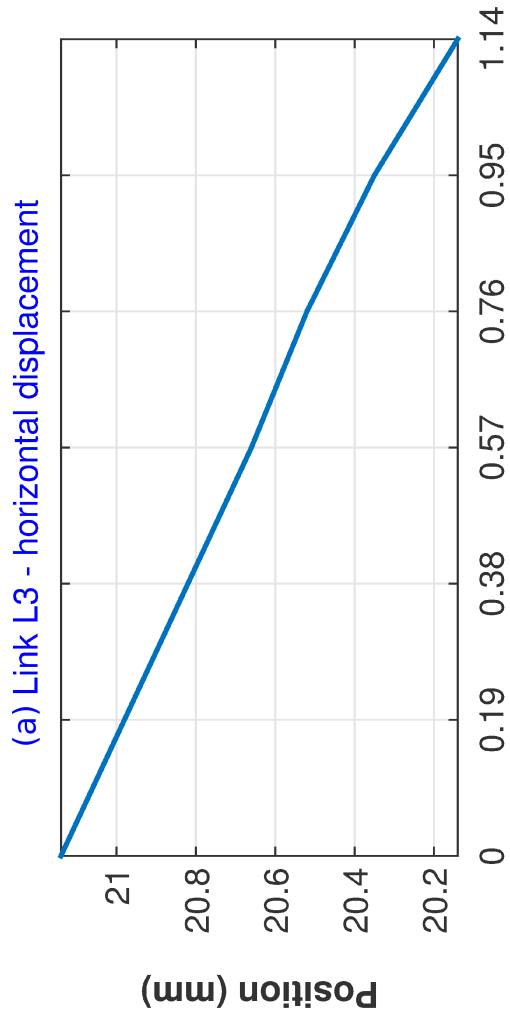
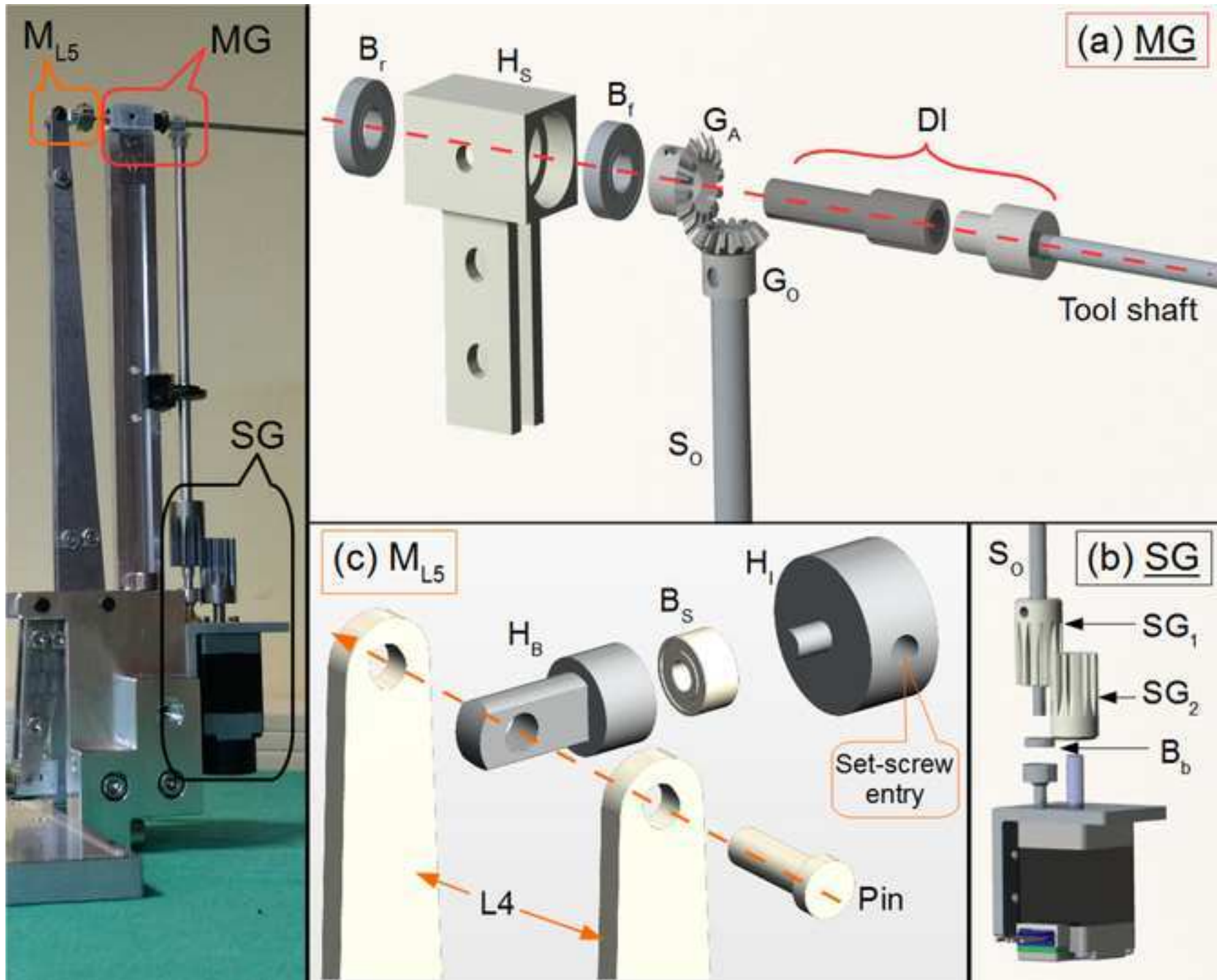


Figure 7





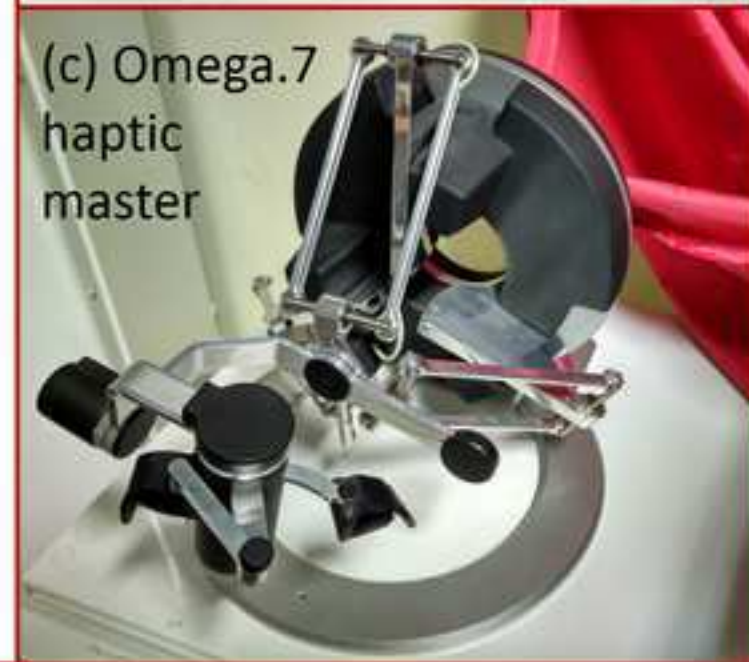
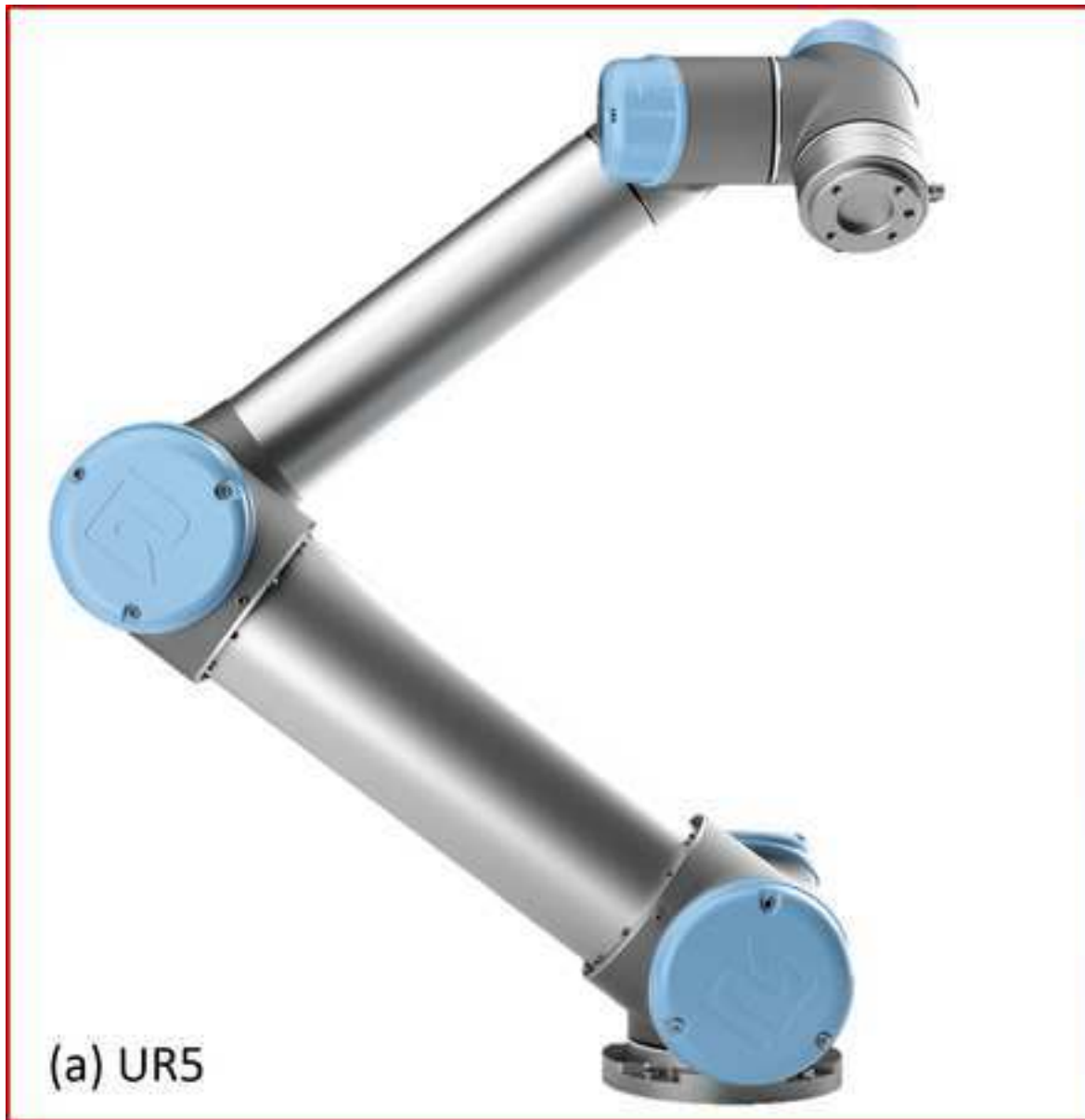


Figure 10

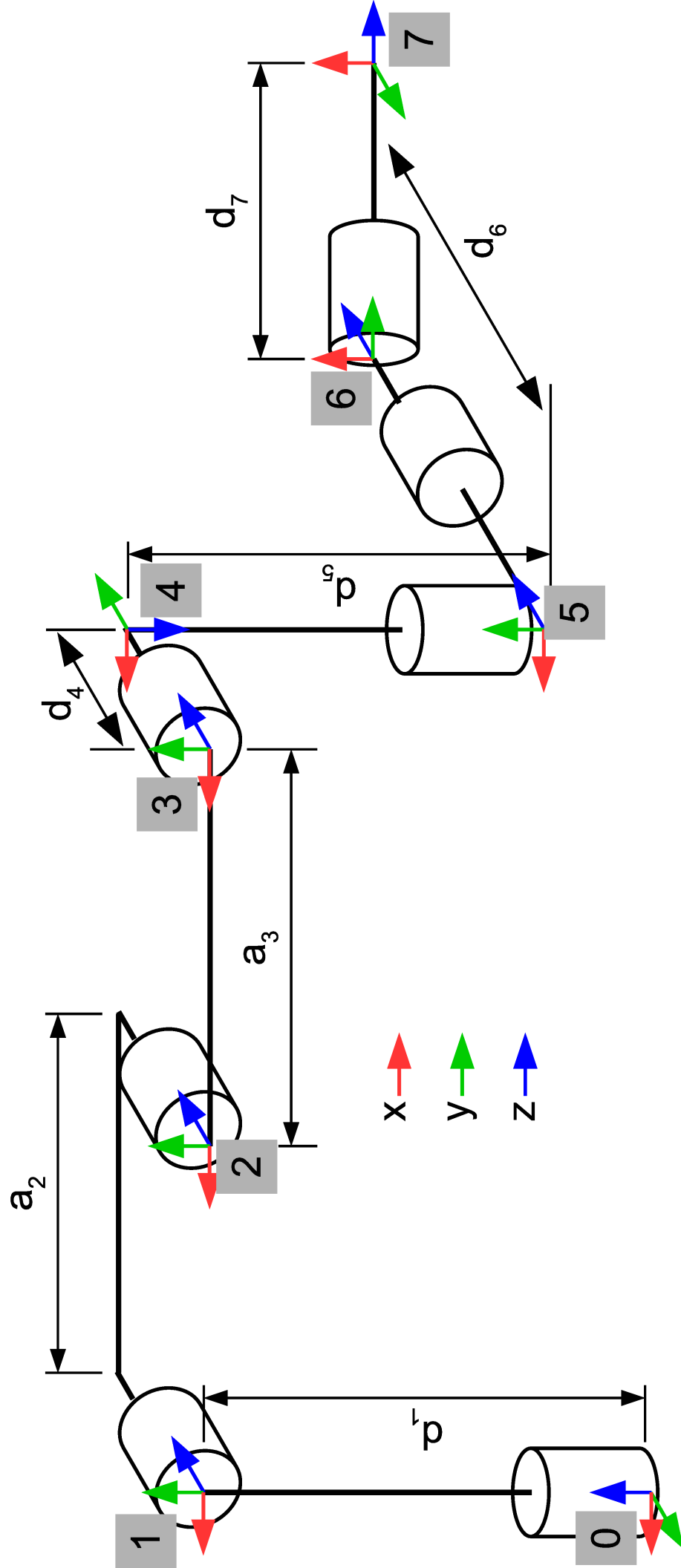
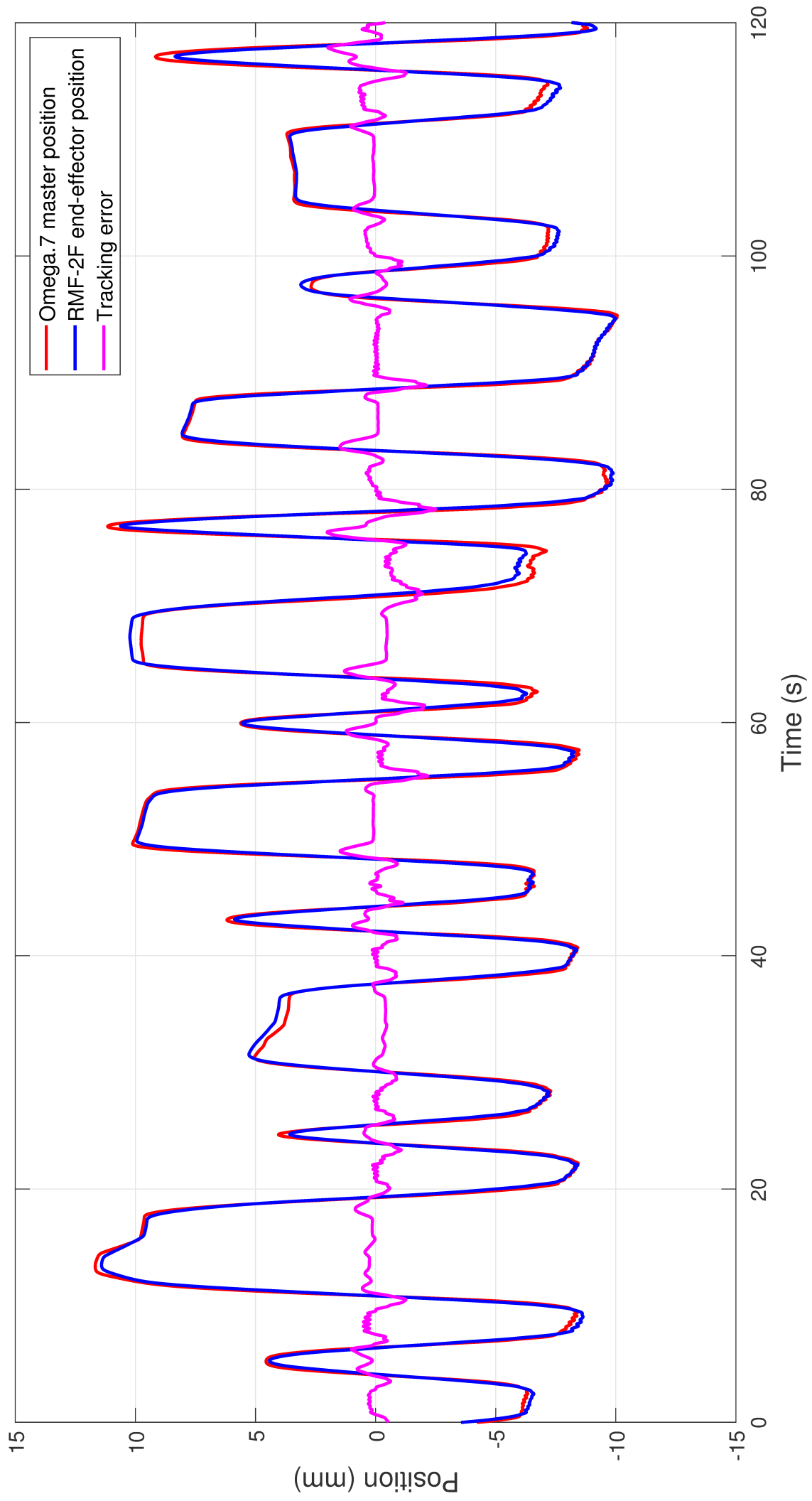


Figure 11



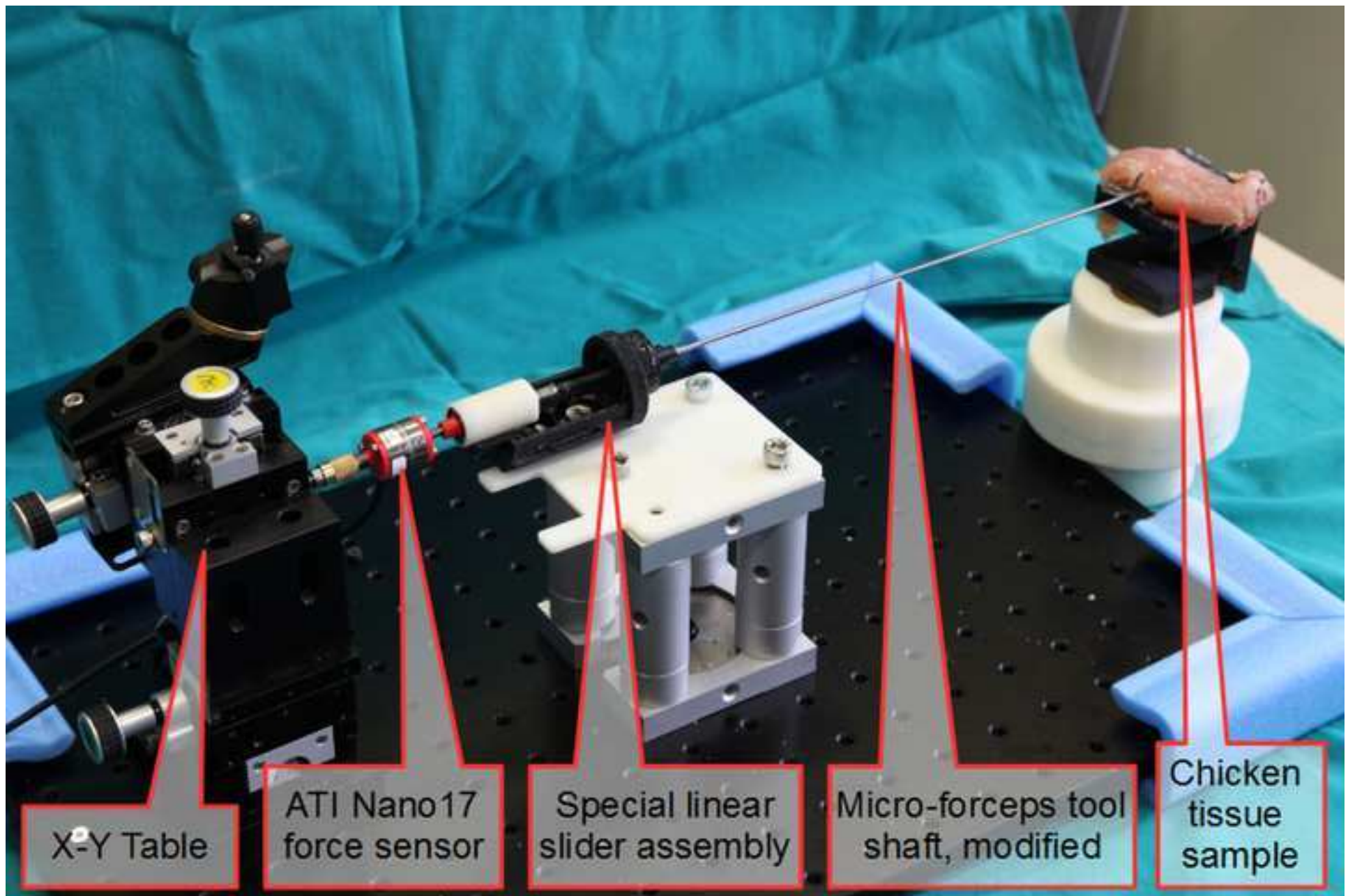
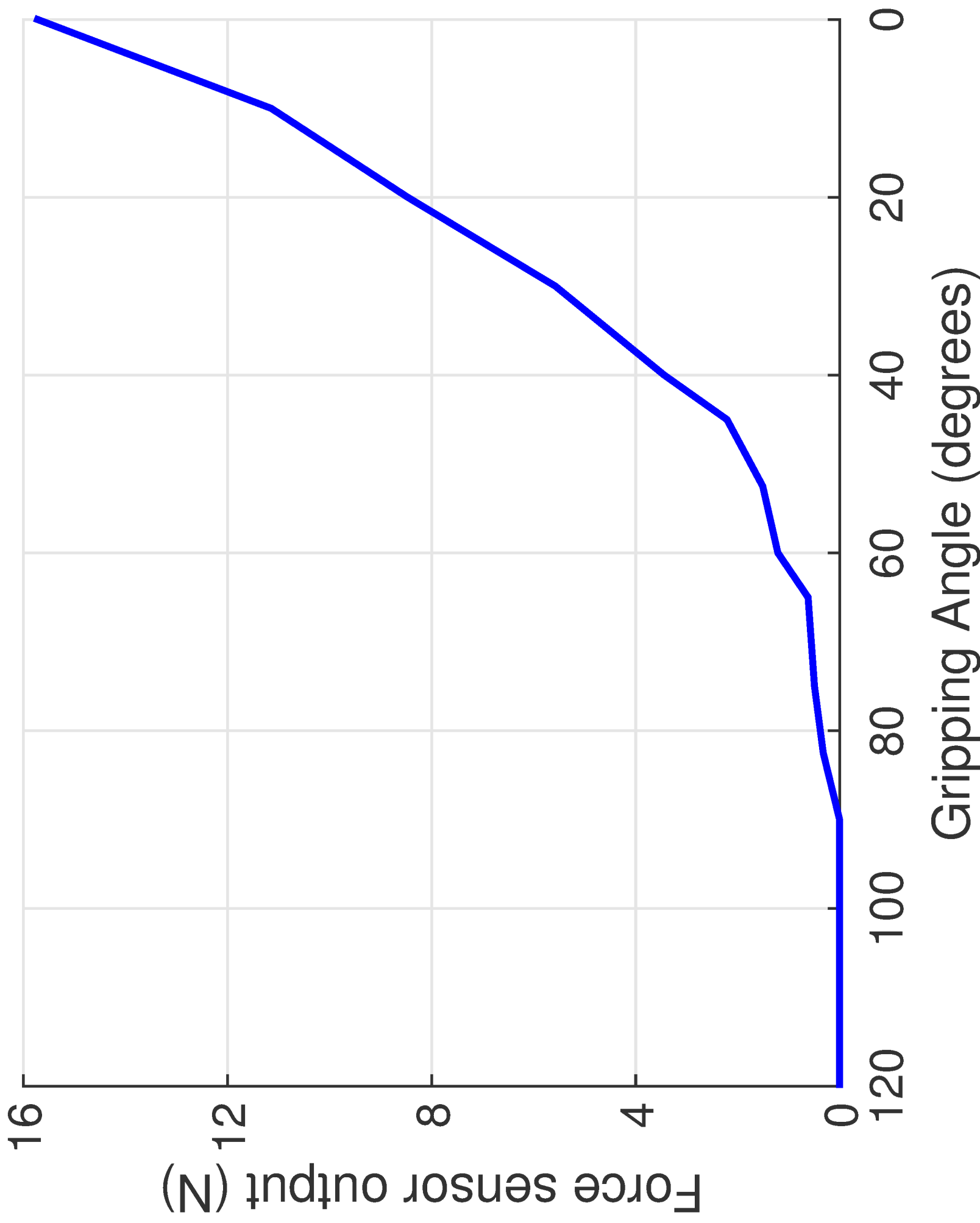


Figure 12b



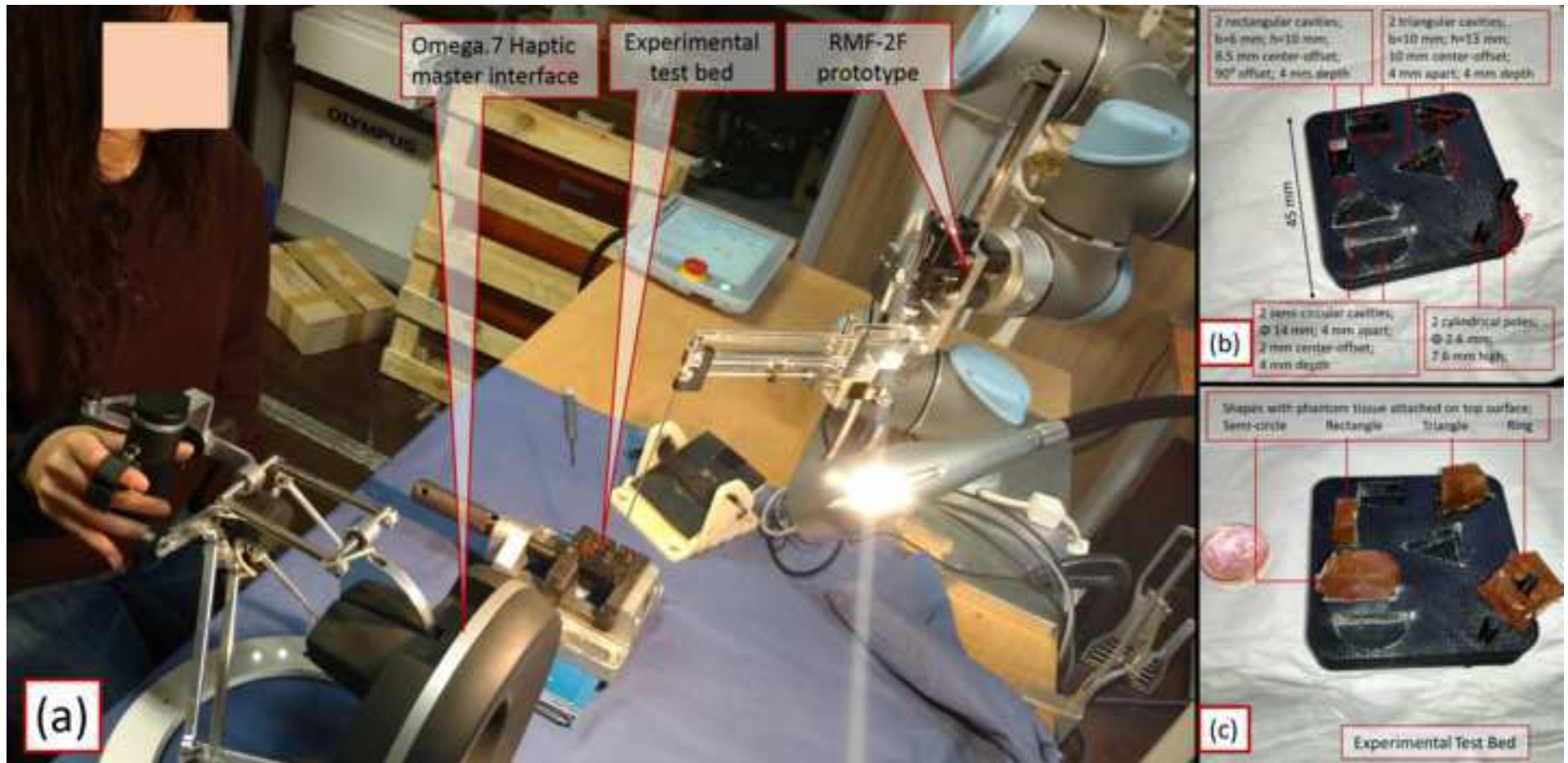


Figure 14

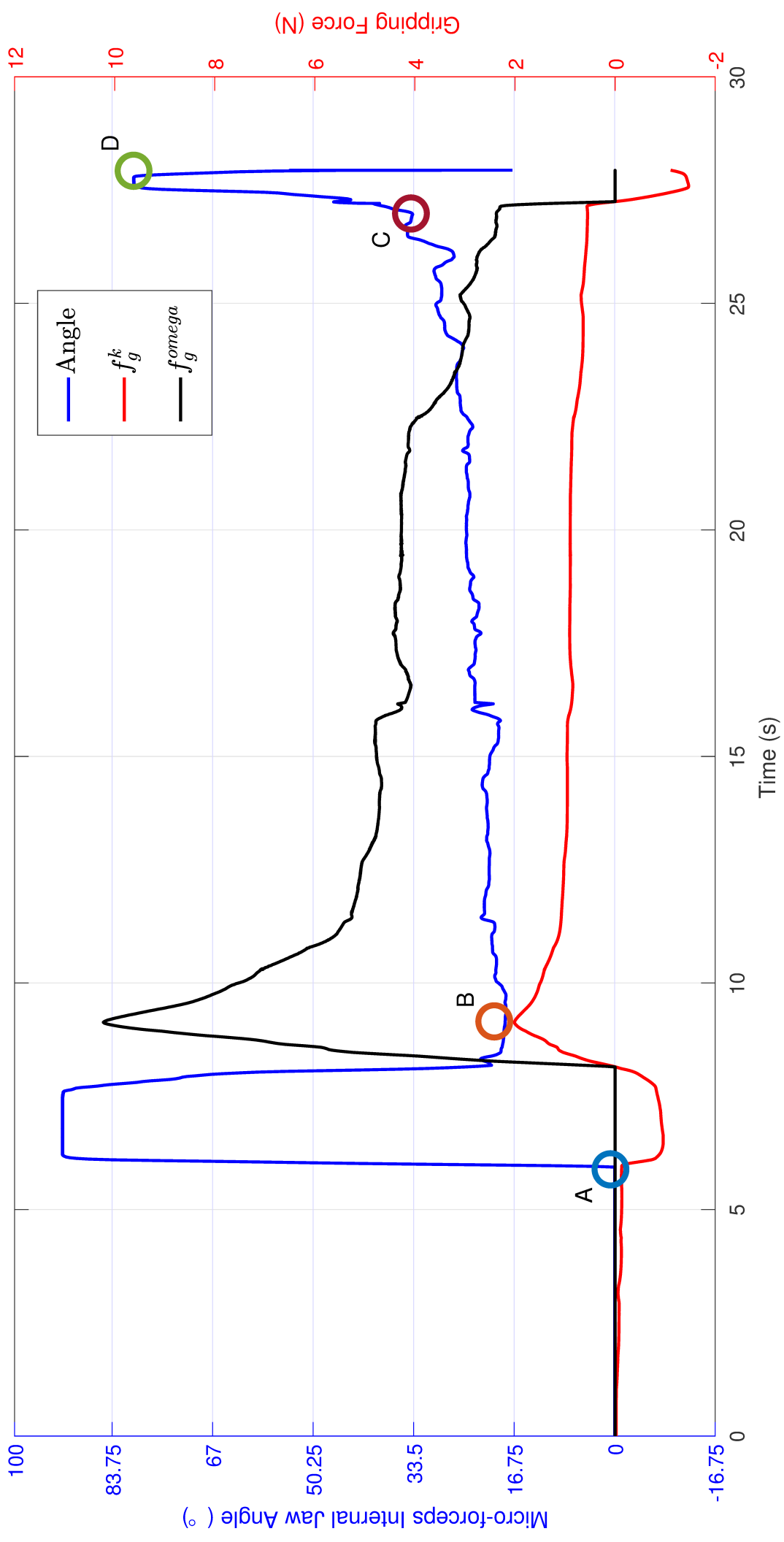


Figure 15a

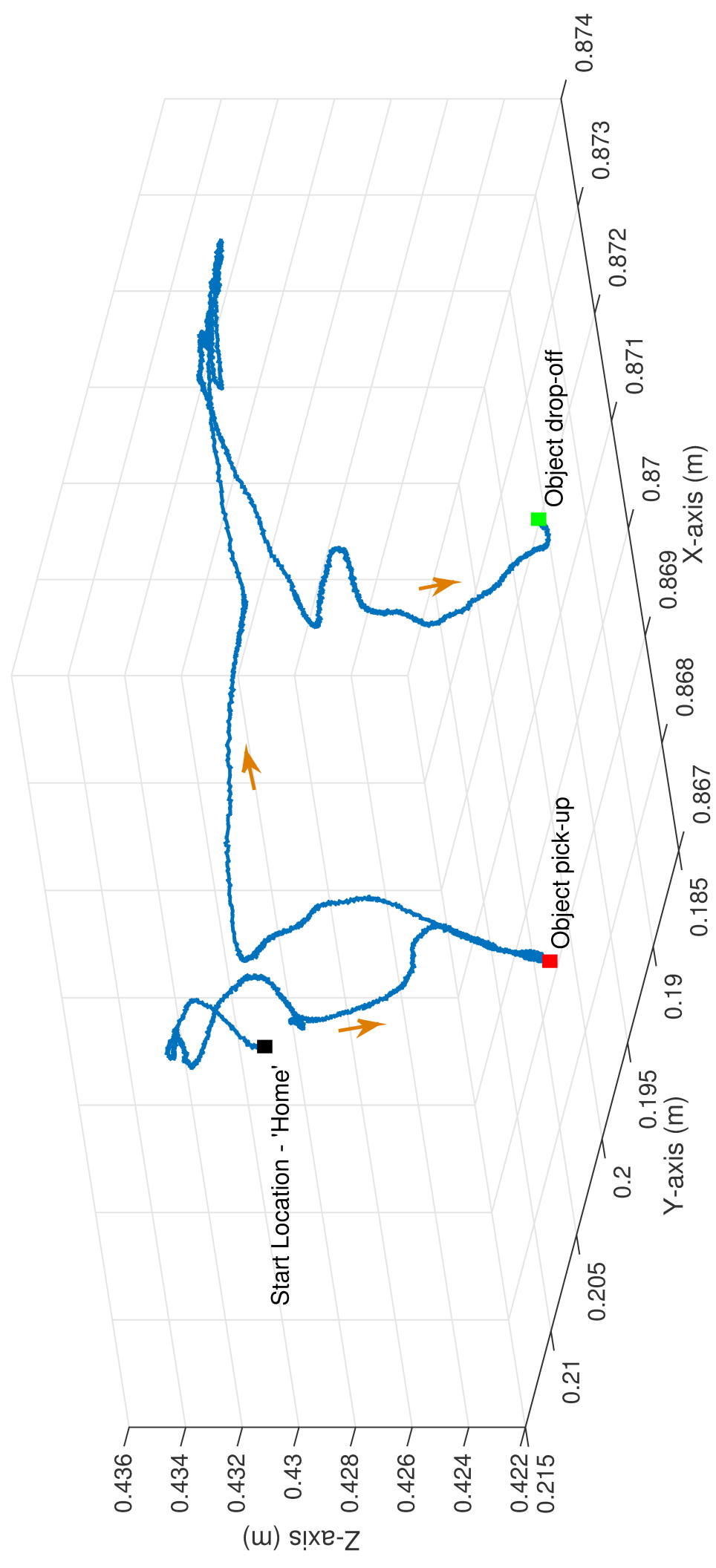


Figure 15b

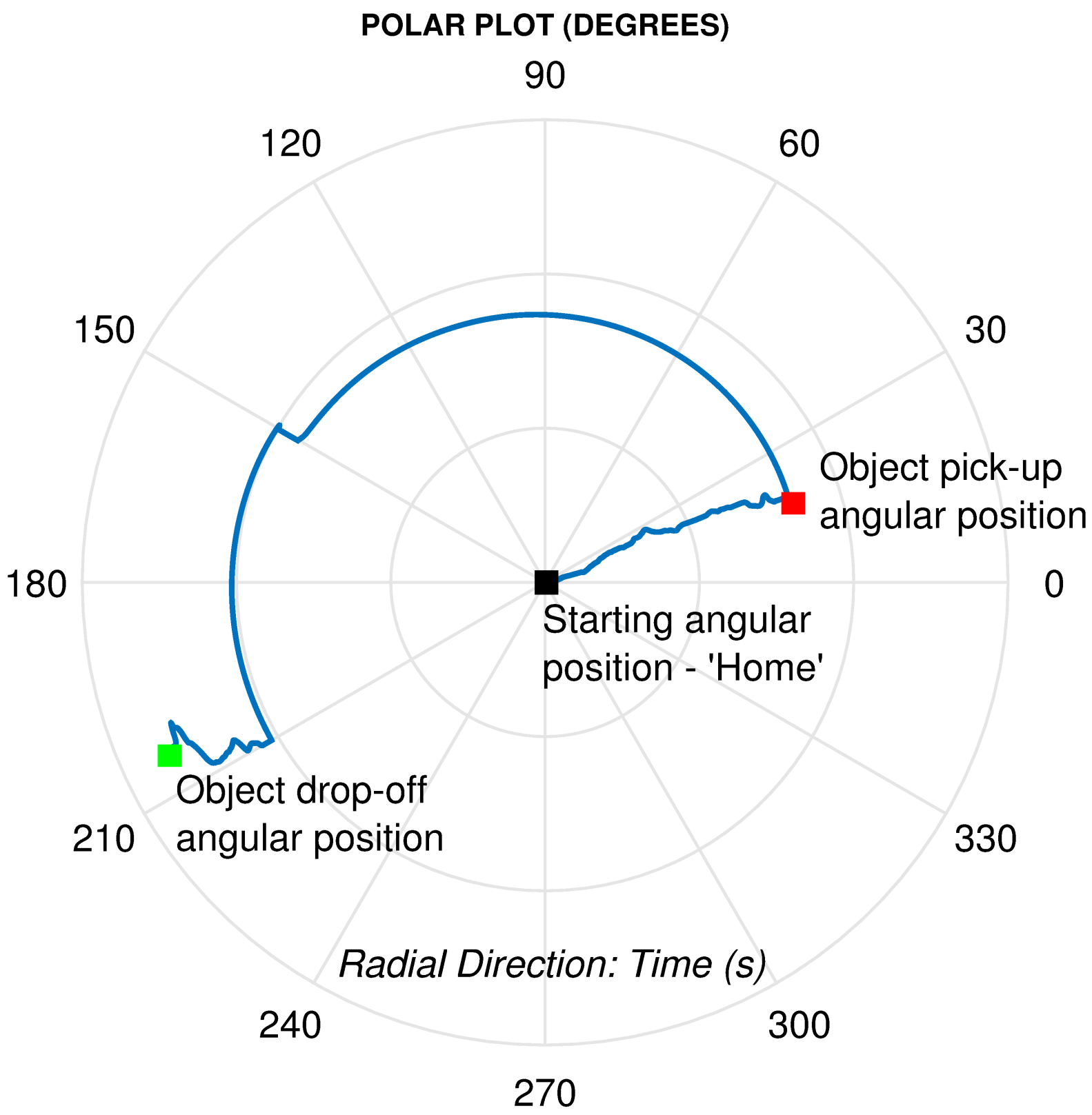


Figure 16a

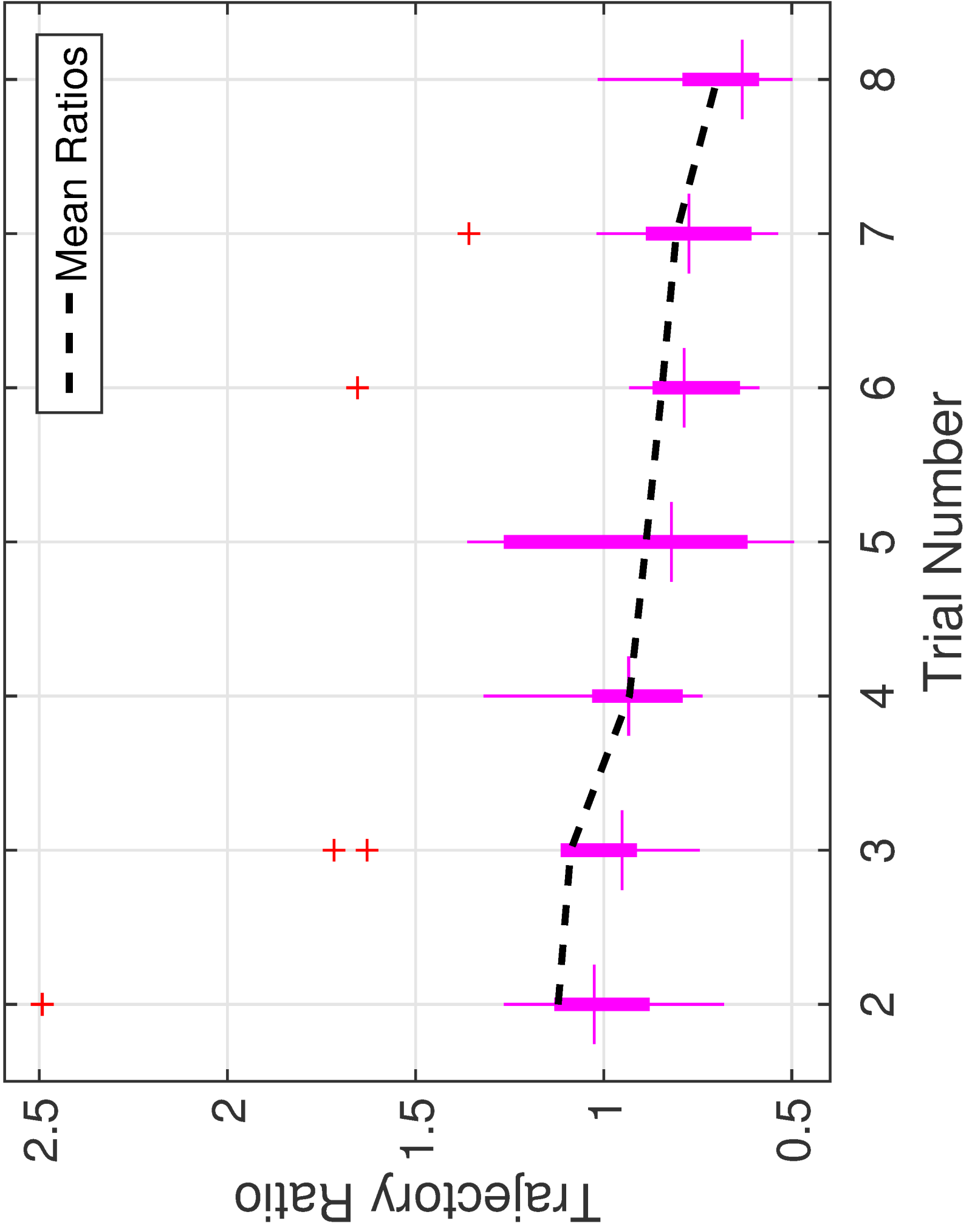


Figure 16b

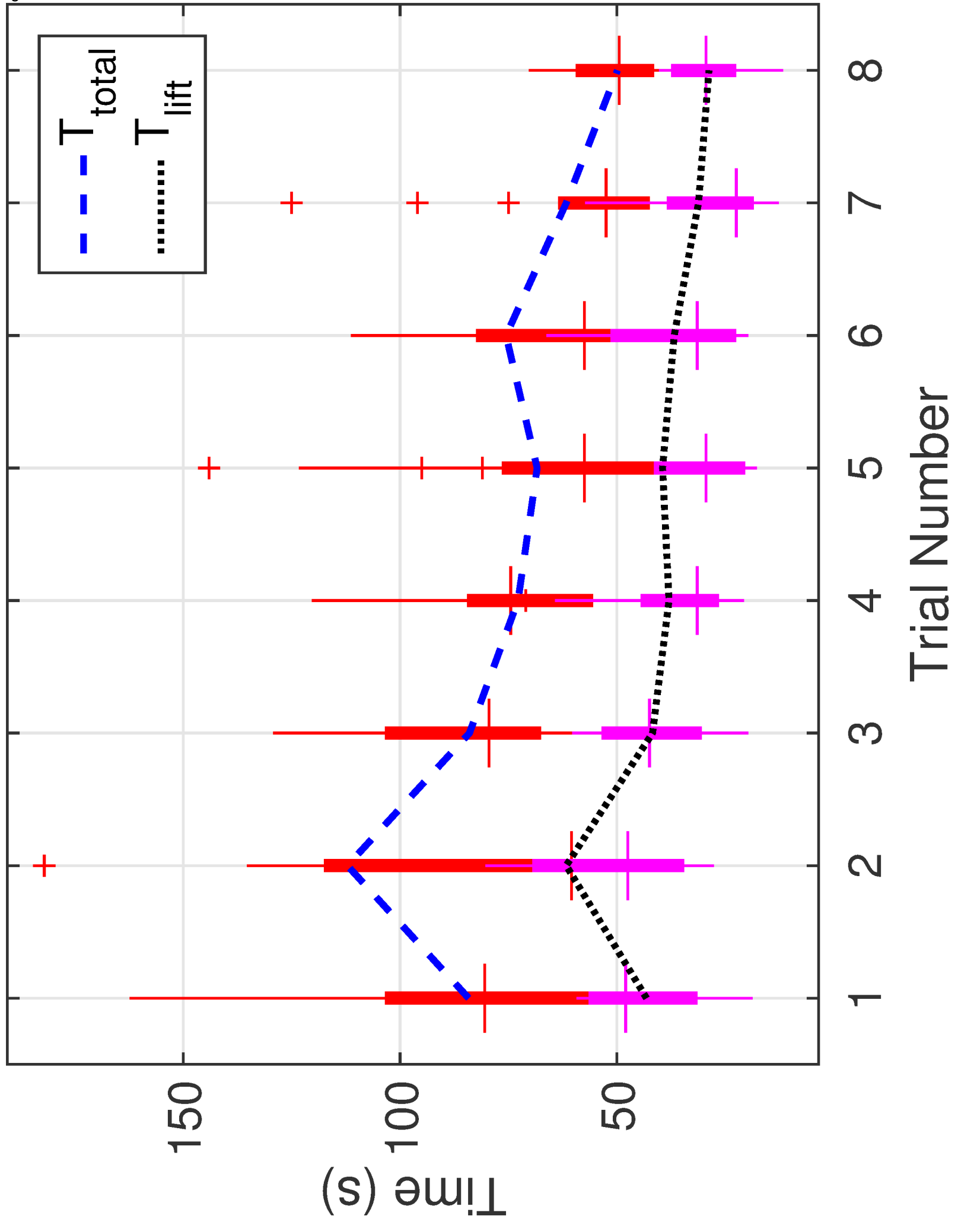


Figure 17a

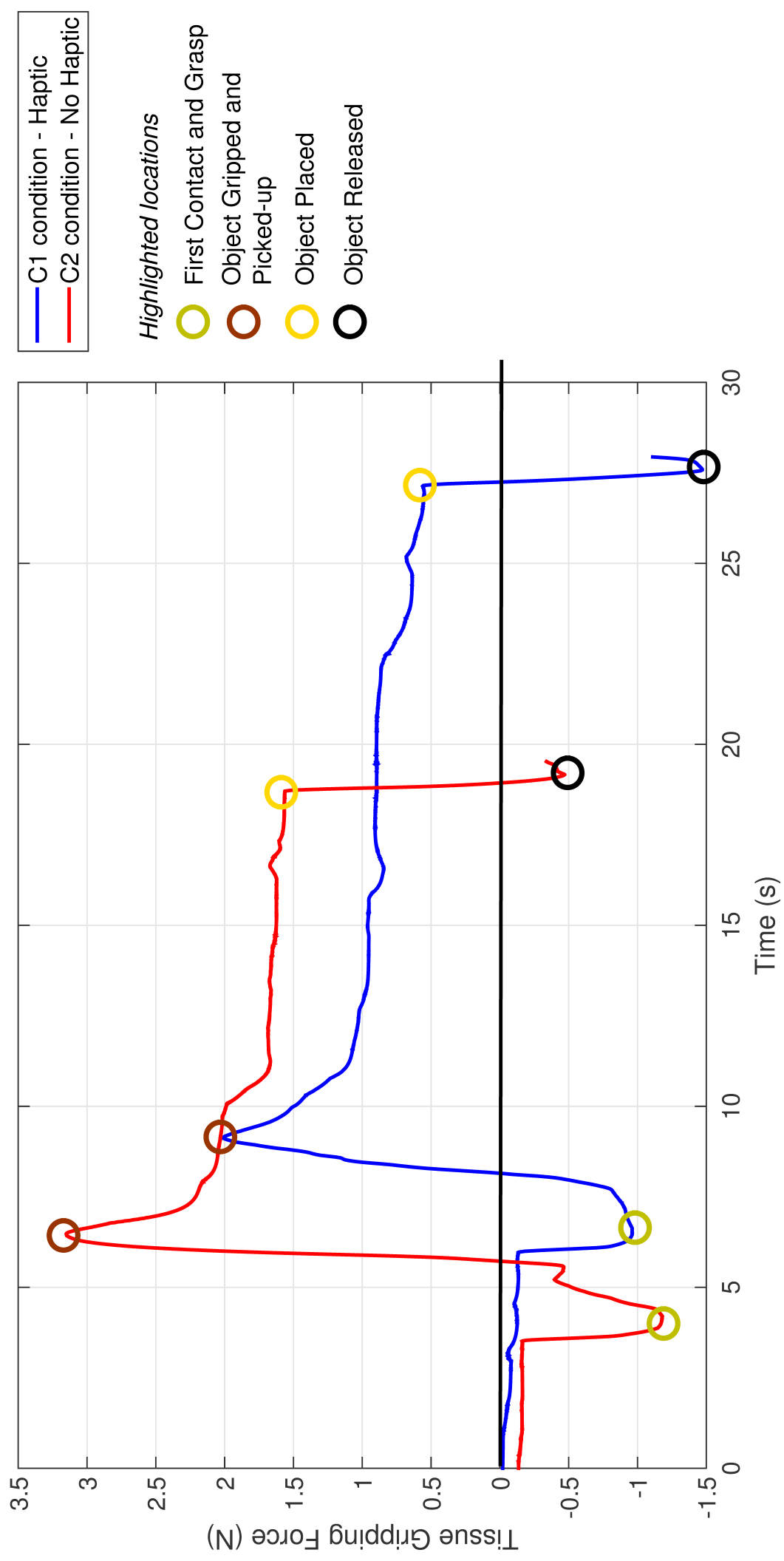
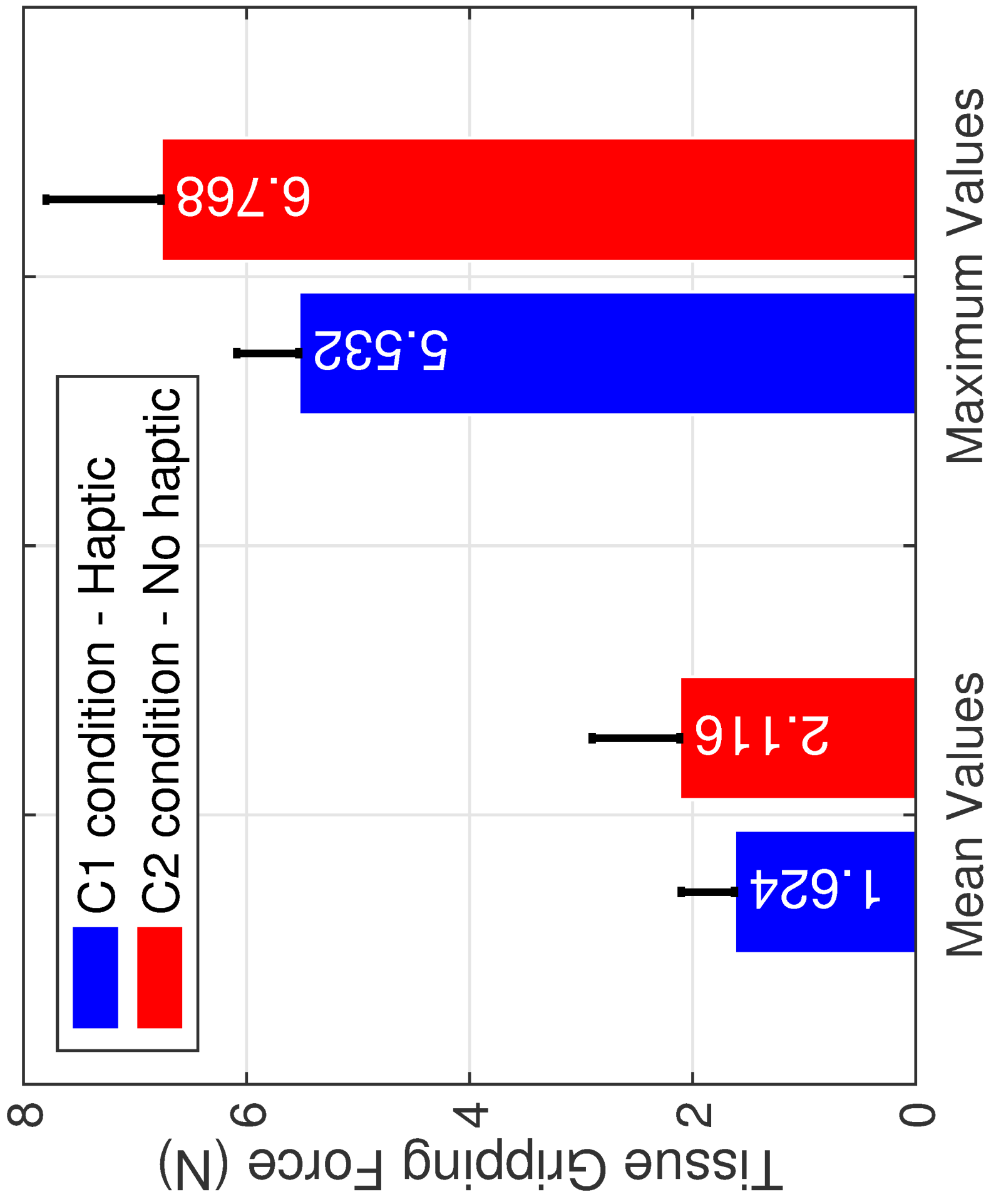


Figure 17b



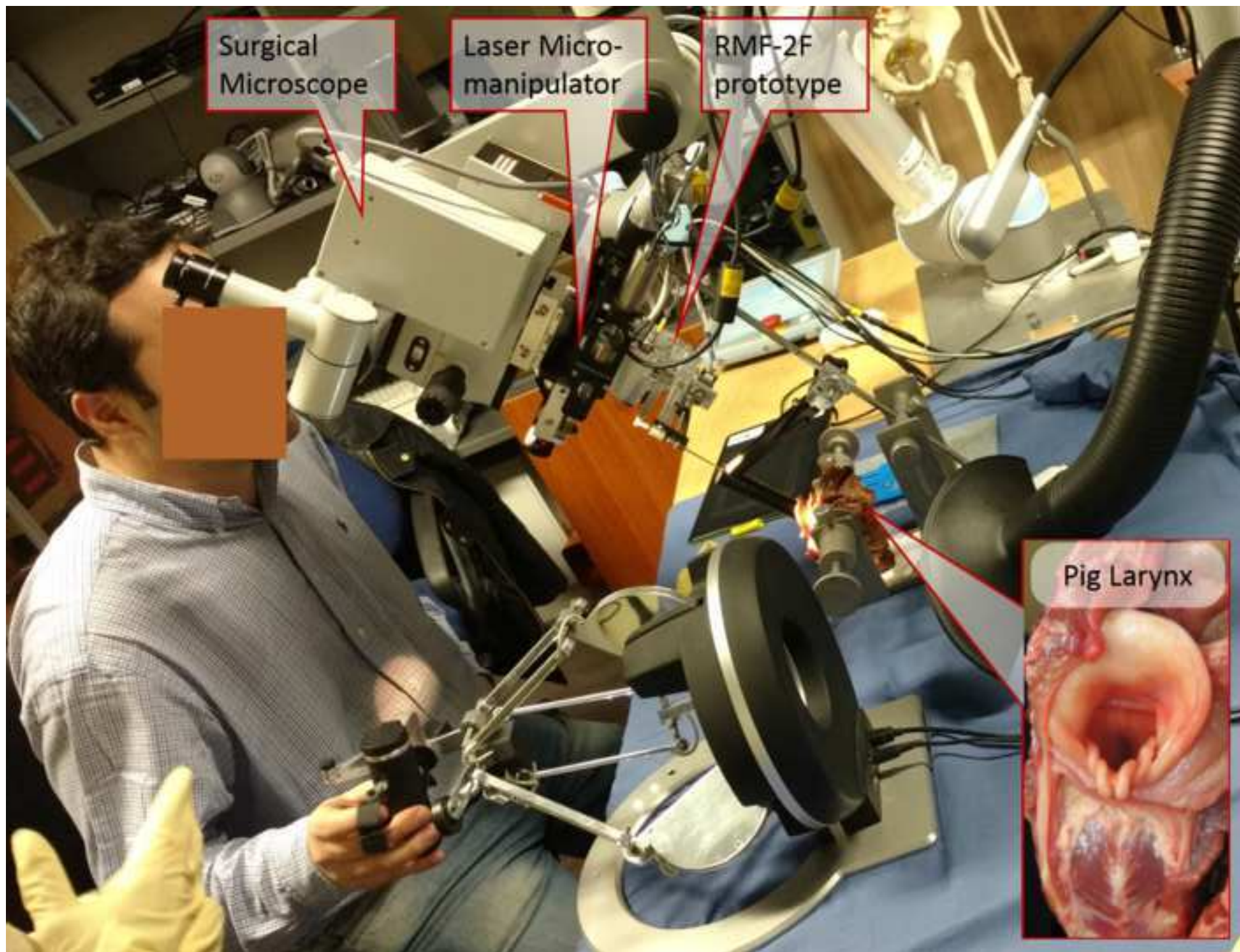


TABLE 1: Design specifications of the microsurgical forceps

Design Needs / Features		Remarks
<b>1.</b>	Displacement from microscope line-of-sight of 200mm.	In order to avoid tool interference with line-of-sight, need to maintain sufficient distance between the tool base and laryngoscope entry point, and minimize surgical vision occlusion.
<b>2.</b>	Tool footprint under the microscope of <10mm.	In order to maintain minimum vision occlusion, when viewed through the microscope.
<b>3.</b>	Introduce tissue surface perception through haptic feedback.	In order to get tissue gripping force feedback.
<b>4.</b>	Enhance the tool capability.	Introduction of tool rotation DOF for enhanced workspace.

TABLE 2: D-H Parameters for the RMF-2F integrated device

Joint	Type	a (m)	$\alpha$ (radians)	d (m)	q (radians)
1	R	0.00000	$\pi/2$	$d_1 = 0.089159$	$q_1$
2	R	-0.42500	0.0	0.0000	$q_2$
3	R	-0.39225	0.0	0.0000	$q_3$
4	F	0.00000	$\pi/2$	$d_4 = 0.10915$	0
5	F	0.00000	$-\pi/2$	$d_5 = 0.09465$	0
6	F	0.00000	0.0	$d_6 = 0.0823 + l_6$	0
7	R	0.00000	$\pi/2$	$d_7 = 0.108 + l_7$	$q_{\text{rot}}$

R = Rotary; F = Fixed.